ARTICLES
https://doi.org/10.1038/s41564-020-00822-7

nature microbiology

The Rcs stress response inversely controls surface and CRISPR–Cas adaptive immunity to discriminate plasmids and phages

Leah M. Smith[1], Simon A. Jackson[1,2], Lucia M. Malone[1], James E. Ussher[1], Paul P. Gardner[2,3,4] and Peter C. Fineran[1,2,4]✉

Bacteria harbour multiple innate defences and adaptive CRISPR–Cas systems that provide immunity against bacteriophages and mobile genetic elements. Although some bacteria modulate defences in response to population density, stress and metabolic state, a lack of high-throughput methods to systematically reveal regulators has hampered efforts to understand when and how immune strategies are deployed. We developed a robust approach called SorTn-seq, which combines saturation transposon mutagenesis, fluorescence-activated cell sorting and deep sequencing to characterize regulatory networks controlling CRISPR–Cas immunity in *Serratia* sp. ATCC 39006. We applied our technology to assess *csm* gene expression for ~300,000 mutants and uncovered multiple pathways regulating type III-A CRISPR–Cas expression. Mutation of *igaA* or *mdoG* activated the Rcs outer-membrane stress response, eliciting cell-surface-based innate immunity against diverse phages via the transcriptional regulators RcsB and RcsA. Activation of this Rcs phosphorelay concomitantly attenuated adaptive immunity by three distinct type I and III CRISPR–Cas systems. Rcs-mediated repression of CRISPR–Cas defence enabled increased acquisition and retention of plasmids. Dual downregulation of cell-surface receptors and adaptive immunity in response to stress by the Rcs pathway enables protection from phage infection without preventing the uptake of plasmids that may harbour beneficial traits.

Bacteria have evolved diverse innate and adaptive defences against mobile genetic elements and phages[1]. The importance of these defences is evident because they can influence the spread of antibiotic resistance genes on mobile elements[2,3] and yet might pose a challenge for the development of phage-based therapies against multi-drug-resistant bacteria[4,5]. To address this challenge, it is paramount to understand when and how bacteria deploy different immune defences. Innate defences include surface modification, restriction modification and abortive infection systems, whereas CRISPR–Cas are the only known adaptive immune systems[1,6]. CRISPR–Cas systems represent a major barrier against different foreign elements by inhibiting both horizontal gene transfer (HGT) and phage infection[2]. These systems capture and store memories of past infections as DNA spacers within CRISPR arrays[7]. CRISPR-associated (Cas) proteins complex with CRISPR-derived RNAs (crRNAs) to form 'interference' complexes that target and degrade complementary nucleic acids, providing immunity[2].

CRISPR–Cas systems vary in genetic organization, interference complex composition, and target recognition mechanisms[8]. Type I and III systems form multi-subunit interference complexes, and target DNA or both DNA and RNA, respectively. Type III systems often co-occur in hosts harbouring type I systems[8,9] and, in some cases, CRISPR–Cas components are shared between systems to generate new memories or provide robustness against immune evasion[10–12]. Unlike type I defence, type III immunity requires target transcription, after which the interference complex binds and cleaves complementary RNA[2]. The large subunit of the complex, Cas10, degrades single-stranded DNA[13] and synthesizes cyclic oligoadenylates, which stimulate non-specific nucleic acid degradation by an accessory nuclease[14–16].

There is little known about if, and how, innate versus CRISPR–Cas adaptive immunity is coordinated to maximize defence and minimize potential costs[17–20]. Regulation studies have predominantly focused on type I systems[21,22] and, despite conferring an advantage over DNA-only targeting systems in clearing some phage infections[10,23,24], few studies have explored how type III activity is regulated[25–27]. Furthermore, networks controlling CRISPR–Cas activity have not been explored in depth for any bacterium, due in part to a lack of scalable methods. In the present study, we developed a genome-wide method (fluorescence-activated cell sorting and transposon insertion sequencing (SorTn-seq)) and comprehensively identified a suite of genes that regulate type III-A CRISPR–Cas expression in *Serratia* sp. ATCC 39006 (hereafter referred to as *Serratia*), a strain also possessing type I-E and I-F systems.

We demonstrate that induction of the Rcs (regulator of capsular polysaccharide synthesis) outer-membrane, stress response pathway represses all three *Serratia* CRISPR–Cas systems, thereby allowing elevated acquisition of antibiotic resistance through conjugation. As Rcs is activated by various stresses, including β-lactam antibiotics[28], we propose that Rcs-mediated repression of CRISPR–Cas enables genetic sampling that may assist bacterial adaptation during stress. Concomitantly, induction of the *Serratia* Rcs response protects cells by upregulating broad-spectrum, innate surface-based phage immunity. Thus, the Rcs pathway inversely coordinates the innate (through surface modification) versus the adaptive arms of the immune response to selectively inhibit different classes of foreign invaders. Our work also highlights the power and general utility of

[1]Department of Microbiology and Immunology, University of Otago, Dunedin, New Zealand. [2]Genetics Otago, University of Otago, Dunedin, New Zealand. [3]Department of Biochemistry, University of Otago, Dunedin, New Zealand. [4]Bio-Protection Research Centre, University of Otago, Dunedin, New Zealand. ✉e-mail: peter.fineran@otago.ac.nz

the SorTn-seq high-throughput technology for probing regulatory networks in bacteria.

Results

SorTn-seq is a powerful tool for regulator discovery. Transcription of the *Serratia* type III-A (*csm*) interference operon initiates from a promoter upstream of *cas10* (Fig. 1a). To find regulators affecting transcription and/or translation of the type III-A interference complex, we constructed a P*csm–eYFP* reporter that includes the *csm* promoter and *cas10* (*csm1*) ribosome-binding site fused to enhanced yellow fluorescent protein (eYFP; Fig. 1b,c), and developed SorTn-seq (Fig. 1d). We generated a high-density transposon (Tn*5* derivative) mutant library and used fluorescence-activated cell sorting (FACS) to sort transposon (Tn) mutants into three bins based on their *csm* expression (eYFP fluorescence): 'low', 'high' and 'depleted'. For each bin, plus unsorted 'input' samples, we performed high-throughput, Tn insertion-site sequencing, and then mapped the Tn insertion sites to the *Serratia* genome (Fig. 1d). Our sequencing depth was sufficient to detect most mutants (Supplementary Fig. 1). Combined, we observed ~293,000 unique Tn insertions (across triplicates), corresponding to a density of 1 per ~17 nucleotides (nt, Fig. 1e). Depleted and input replicates contained >100,000 unique insertions, whereas each high and low samples contained ~30,000 unique insertions (Fig. 2a and Supplementary Table 1).

To identify host-encoded *csm* regulators, we compared unique insertions per gene/feature using an exact test for differential expression on data fit to a negative binomial distribution model[29]. The biological coefficient of variation (BCV)[29] was similar between samples from the three independent sorts (Fig. 2b), indicating reproducible enrichment by cell sorting and sequencing of mutants with altered reporter expression. Potential regulators were features significantly (P (adjusted) < 0.05) enriched in the high or low bins, relative to the depleted samples (Fig. 2c,d and Supplementary Data file 1). Using this approach, we identified 31 gene features enriched in the low expression bin and 30 in the high bin (Supplementary Table 2), indicating their potential role in *csm* activation or repression, respectively.

In addition, our analysis revealed significant enrichment of several intergenic regions (eight in low and three in high; Supplementary Data File 1). To assess the validity of regulator prediction, we confirmed multiple top hits by measuring *csm* expression in 21 individual deletion or Tn mutant strains (Fig. 2e and Supplementary Table 3). For these mutants, decreases or increases in *csm* expression (Fig. 2e) were consistent with the enrichment of Tn insertions in these genes within the appropriate low or high bin (Fig. 2c,d). We identified multiple signalling pathways and regulators that modulate type III-A *csm* expression (Fig. 2c,d, Extended Data Fig. 1 and Supplementary Table 2), including metabolic regulators such as the Rsm (regulator of secondary metabolism) system and the cAMP-receptor protein (CRP)–cAMP complex. Other mutations identified implicate motility and stress responses as important modulators of CRISPR–Cas. These findings and others are discussed in detail in the Supplementary Discussion. In summary, SorTn-seq is a powerful, high-throughput, forward genetic screening platform for the identification of regulators of bacterial gene expression.

The Rcs membrane-stress response pathway regulates type III CRISPR–Cas expression. Of all strains tested, mutation of the *igaA* gene had the strongest effect on *csm* expression (Fig. 2e). IgaA is a membrane-bound repressor of the Rcs phosphorelay signalling cascade, a stress response pathway first characterized as a regulator of capsular polysaccharide synthesis in *Escherichia coli*[30]. The Rcs phosphorelay is inhibited by IgaA until a stress-induced interaction occurs with the outer-membrane lipoprotein RcsF[31–34] (Fig. 3a). De-repression of the RcsC histidine kinase activity leads

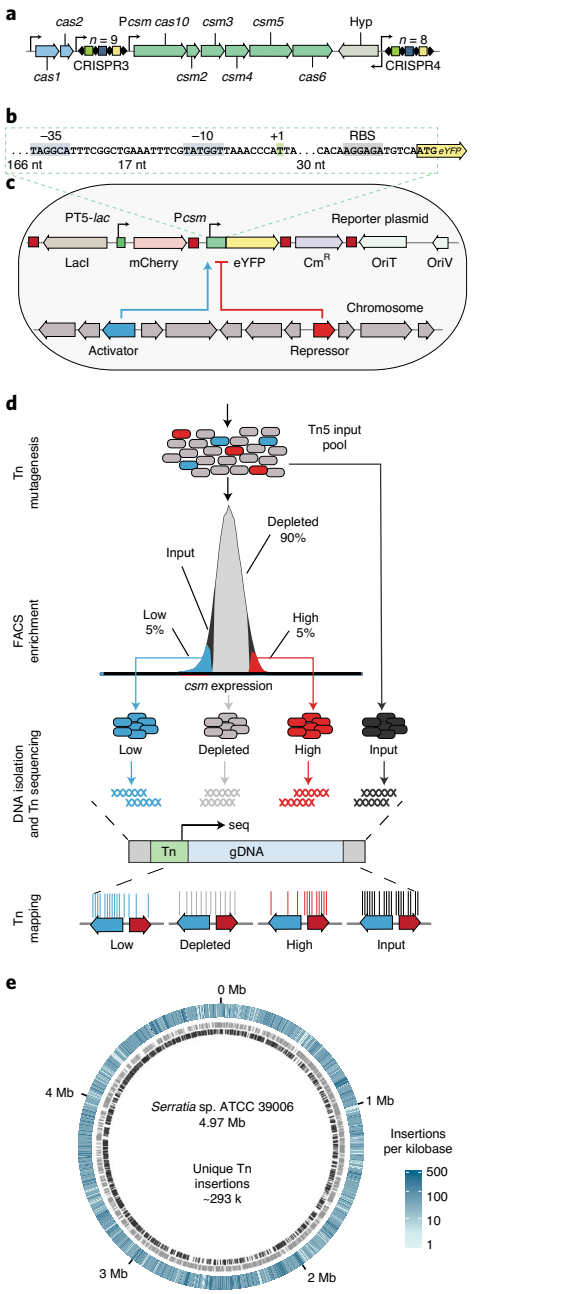

Fig. 1 | Overview of the type III-A *csm* promoter, fluorescent reporter plasmid and high-throughput SorTn-seq workflow. a, The type III-A CRISPR–Cas system of *Serratia*. **b**, Expression of *csm* during SorTn-seq was measured from an eYFP fusion to 250 nt upstream of *cas10*. This region contains a promoter for the entire type III-A interference (*csm*) operon. Key features are indicated, including promoter elements (−35 and −10; blue boxes), transcription start site (+1; green box), RBS (grey box). **c**, Plasmid map of the P*csm–eYFP* reporter with major features indicated. Dark-red boxes are transcriptional terminators. The plasmid contains an IPTG-inducible mCherry gene which is used as a proxy for cell health/plasmid copy number. Chromosomally encoded activators (blue) or repressors (red) influence levels of the *csm–eYFP* reporter. **d**, Overview of the SorTn-seq method. Cells harbouring the *csm–eYFP* reporter are subjected to Tn mutagenesis and sorted based on fluorescence levels. DNA is extracted from sorted populations and Tn insertion sequencing is employed to locate insertions influencing *csm* expression. gDNA, genomic DNA. **e**, The *Serratia* genome displaying Tn insertion density (outer ring) and genes on the forward (grey) and reverse (black) strands.

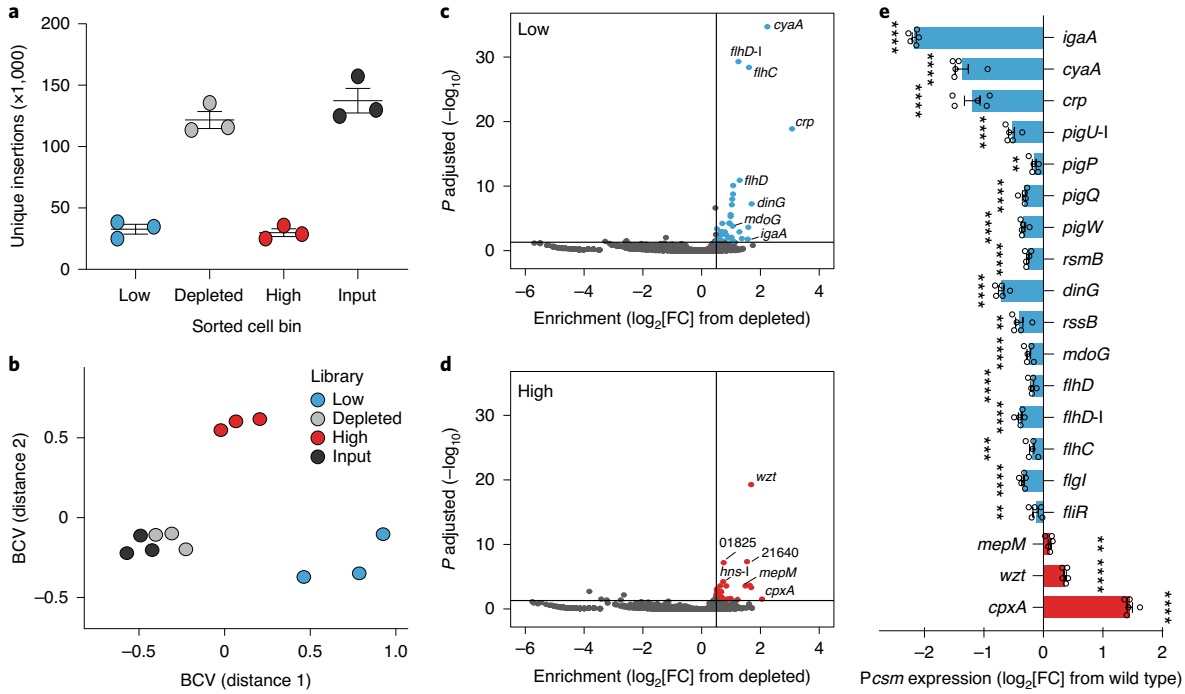

Fig. 2 | SorTn-seq reveals type III-A CRISPR–Cas regulators. a, Unique Tn mutants observed in each sorted bin ($n = 3$ independent sorts; lines represent the mean and s.e.m.). Insertion count data are summarized in Supplementary Table 1. **b**, The BCV between sample replicates, based on the top 100 most variable features. **c**,**d**, Significant enrichment of mutants in low (**c**) and high (**d**) samples compared with the depleted controls, as determined via an exact test for differential expression using edgeR[29]. Horizontal lines indicate a *P* value of 0.05 (adjusted for multiple comparisons using the Benjamini–Hochberg FDR correction); vertical lines indicate a $\log_2$ fold change of 0.5. FC, fold change. Classification of significantly enriched genes is outlined in Supplementary Table 2. **e**, Validation of *csm* expression in individual mutant strains. Mutations in *csm* activators are shown in blue and repressors in red ($n = 5$ biologically independent samples). All bars represent the mean and error bars the s.e.m. Expression and enrichment data for strains in **e** and for additional strains are summarized in Supplementary Table 3. Two-sided Student's *t*-tests were used to determine statistical significance. Detailed statistical testing can be found in the accompanying Source data. $^{****}P < 0.0001$; $^{***}P < 0.001$; $^{**}P < 0.01$.

to RcsD-mediated phosphorylation of RcsB, which dimerizes and directly regulates gene expression (Fig. 3a). In agreement, deletion of *rcsB* or *rcsD* restored *csm* expression in the *igaA* mutant to wild-type levels (Fig. 3b). Repression of *csm* expression in the *igaA* strain was confirmed using a chromosomal *csm–lacZ* translational fusion (Extended Data Fig. 2a). Furthermore, expression of *igaA* in trans complemented *csm* expression levels in the *igaA* mutant (Extended Data Fig. 2b).

RcsB can also form DNA-binding heterodimers with accessory proteins[35], including RcsA, a positive regulator of capsule synthesis[36,37]. The most similar RcsA homologue in *Serratia* is a LuxR-family transcriptional regulator (RS09790; Extended Data Fig. 2c) with 29% amino acid identity to *E. coli* RcsA. Consistent with a role as an RcsB partner, deletion of *rcsA* restored *csm* expression in the *igaA* mutant (Fig. 3b). Furthermore, double mutation of *rcsA* and *rcsB* was similar to either single mutation, with respect to restoration of *csm* expression, supporting their role in repression (Fig. 3b). In *E. coli*, expression of *rcsA* is repressed by H-NS[38] but positively autoregulated by RcsB and RcsA[39]. In agreement, we observed an upregulation of *rcsA* expression in the *igaA* mutant (Extended Data Fig. 2d).

A reliable measure of Rcs activation is increased expression of *rprA* (RpoS regulator), a non-coding RNA that enhances turnover of the sigma factor RpoS[40,41]. Indeed, *rprA* expression was elevated in the *igaA* mutant and was dependent on *rcsB* (Fig. 3c)—consistent with *rprA* activation via the RcsB homodimer in *E. coli*[41]. It is interesting that deletion of *rprA* in the *igaA* background did not affect *csm* expression, indicating that CRISPR–Cas repression is independent of *rprA* (Fig. 3d). Taken together, activation of the Rcs stress response represses type III-A CRISPR–Cas expression and requires both RcsB and RcsA transcriptional regulators.

Mutations that induce the Rcs pathway regulate type III CRISPR–Cas. SorTn-seq identified additional genes involved in the induction of Rcs signalling, including *mdoG* and *mdoH* (Fig. 3e, Supplementary Table 2 and Supplementary Data File 1), which form an operon that controls glucose polymer synthesis in the envelope of enterobacteria[42,43]. These oligosaccharides, which are also known as osmoregulated periplasmic glucans, serve as important determinants of virulence and motility, and are modulated in response to changes in osmolarity[43,44]. Mutation of *mdoG* or *mdoH* leads to loss of periplasmic oligosaccharides, which activates the Rcs stress response pathway[45–49]. Likewise, moderate *csm* repression in a *Serratia mdoG* mutant was dependent on the Rcs pathway (Fig. 3b). Similar to the *igaA* mutant, *rprA* expression was enhanced in the *mdoG* mutant (Fig. 3c), and deletion of *rprA* did not restore *csm* expression (Fig. 3d).

Activation of the Rcs pathway often requires RcsF, a lipoprotein that normally associates with outer-membrane proteins (OMPs)[50] in an interaction facilitated by the β-barrel assembly machine (Bam) complex[32,51]. In *E. coli*, mutation of *bamE* severely diminishes RcsF/OmpA complex formation, which is required for RcsF to sense stresses such as mutations in genes encoding lipopolysaccharide (LPS)[52]. In addition to the *mdoGH* operon, mutations were also enriched in an orthologue of *bamE* in the low *csm* bin (Fig. 3e and Supplementary Data File 1). Although BamA–E were essential for *Serratia* growth, mutation of this BamE orthologue may prevent association of RcsF with OMPs, resulting in activation of the

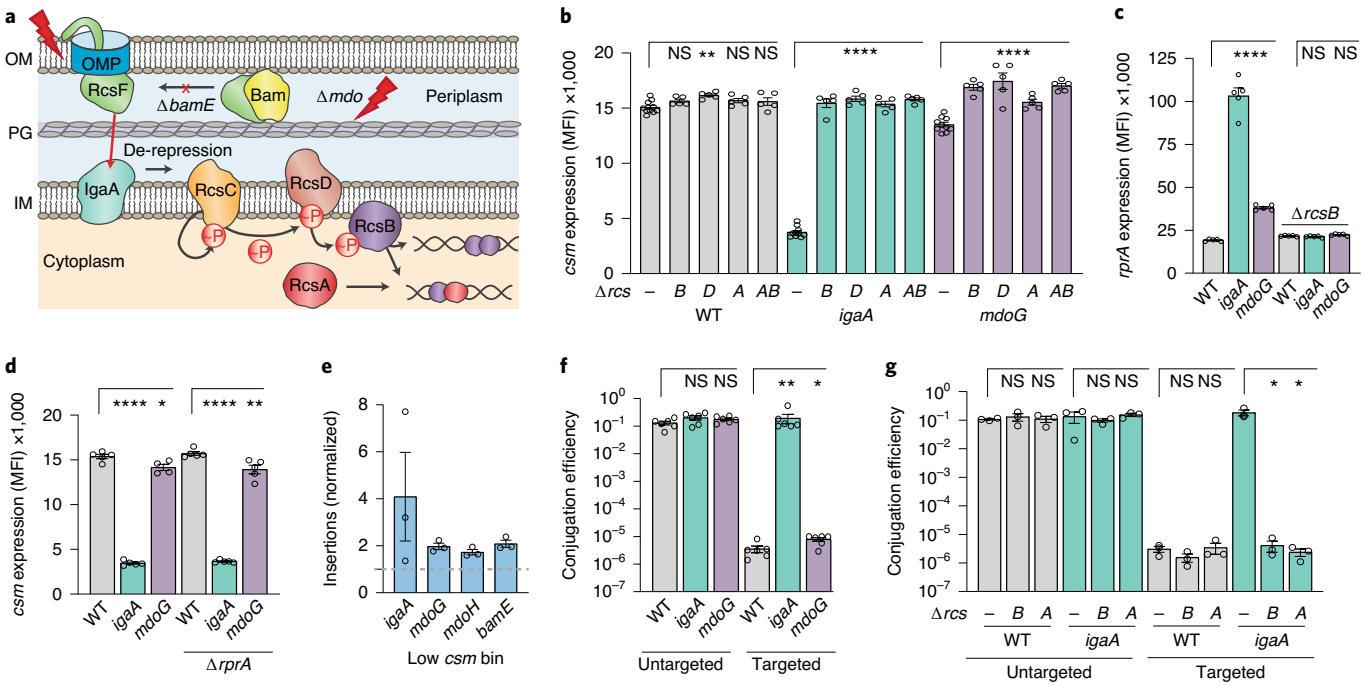

Fig. 3 | Rcs pathway activation represses type III CRISPR–Cas activity. a, The Rcs system responds to extracytoplasmic stress. The Bam complex machinery facilitates the association of lipoprotein RcsF with OMPs. Outer membrane (OM), periplasmic, inner membrane (IM) or peptidoglycan (PG) stress (red arrows) is transduced from RcsF to repressor IgaA, which leads to de-repression of the downstream cascade. RcsC autophosphorylates and transfers phosphate to RcsD, which is transferred to RcsB. RcsB dimerizes with itself or accessory proteins, including RcsA, to regulate target transcription. **b**, Deletion of Rcs components restores *csm* expression to WT levels (median fluorescence intensity (MFI) is in arbitrary units; $n = 5$ biologically independent samples). **c**, Expression of the small RNA *rprA* is elevated in *mdoG* and *igaA* deletion backgrounds, and restored upon *rcsB* deletion, indicating activation of the Rcs pathway ($n = 5$ biologically independent samples). **d**, Repression of *csm* expression in Rcs strains is independent of levels of *rprA* ($n = 5$ biologically independent samples). **e**, Number of insertions in *igaA, mdoG, mdoH* and *bamE* within the low bins, relative to depleted (normalized to 1; grey line; $n = 3$ independent sorts). **f**, Type III-A CRISPR–Cas interference measured through conjugation efficiency of a plasmid carrying a protospacer matching the endogenous CRISPR3 array (targeted) or control (untargeted) ($n = 6$ biologically independent samples). **g**, Reduction of type III-A CRISPR–Cas interference in strain *igaA* is dependent on both *rcsA* and *rcsB* ($n = 6$ biologically independent samples). All bars represent the mean and error bars the s.e.m. To determine statistical significance, two-sided Student's *t*-tests were used for **b**, **c** and **d**, and Mann–Whitney *U*-tests for **f** and **g**. Detailed statistical testing can be found in the accompanying Source data. $^{****}P < 0.0001$; $^{**}P < 0.01$; $^{*}P < 0.05$; NS, not significant.

phosphorelay via de-repression of IgaA through an accumulation of periplasmic RcsF[32,52].

In addition, four genes and one intergenic region within a putative *rfb* O-antigen biosynthetic locus[53] were enriched within the low *csm* bin (Supplementary Table 2 and Supplementary Data File 1). LPS mutations are known to induce Rcs signalling in *E. coli*[54,55]. Therefore, changes in LPS structure may similarly activate the Rcs pathway in *Serratia*[52]. Thus, SorTn-seq has identified several factors known to induce Rcs signalling, activation of which results in *csm* repression.

The Rcs pathway regulates type III CRISPR–Cas interference. Next, we determined whether Rcs-mediated repression of type III-A *csm* genes altered CRISPR–Cas-mediated immunity. We exposed *Serratia* to a foreign plasmid encoding chloramphenicol resistance and introduced this by conjugation. A control plasmid containing no complementarity to spacers in the type III CRISPR3 or CRISPR4 arrays (Fig. 1a) transferred chloramphenicol resistance efficiently into all strains (~10^{-1}; Fig. 3f, untargeted). In contrast, robust immunity was observed in the wild-type against a plasmid containing a sequence targeted by a type III spacer (~10^{-6}; Fig. 3f, targeted). Strikingly, immunity was completely abolished in the *igaA* mutant, showing that this mutation lowered interference by ~10^5-fold relative to the wild-type, and allowed acquisition of antibiotic resistance. Activation of the Rcs pathway through mutation of *mdoG* also reduced interference, but more subtly than the *igaA* mutant (~5-fold; Fig. 3f)—consistent with the magnitude of *csm* expression changes. In agreement with restoration of *csm* expression levels on deletion of *rcsB* or *rcsA* (Fig. 3b), CRISPR–Cas immunity against targeted plasmids was restored on deletion of these regulators in the *igaA* background (Fig. 3g). Overall, activation of the Rcs envelope stress response strongly represses type III CRISPR–Cas expression and interference, and therefore allows cells to acquire foreign genetic material via conjugation, such as antibiotic resistance genes.

Rcs signalling represses multiple distinct CRISPR–Cas systems. In addition to the type III-A system, *Serratia* possesses type I-E and I-F CRISPR–Cas systems (Fig. 4a,b). We hypothesized that the Rcs pathway may coordinately regulate all three CRISPR–Cas systems, which is a phenomenon we previously observed for quorum-sensing control of adaptive immunity[56]. Indeed, expression of the type I-E and I-F *cas* operons (*cas3* and *cas1* reporters, respectively) was reduced in the *igaA* mutant (Fig. 4c,e). Furthermore, mutation of *mdoG* significantly affected type I-E expression, but not type I-F (Fig. 4c,e). Deletion of *rcsB* and *rcsD* restored expression of *cas3* (type I-E) and *cas1* (type I-F), with partial (*cas3*) or full (*cas1*) restoration on deletion of *rcsA* alone (Extended Data Fig. 3a,b). As with the type III-A system, *rprA* did not contribute to Rcs-mediated type I repression (Extended Data Fig. 3a,b).

Next, we tested the effect of *igaA* and *mdoG* mutations on type I CRISPR–Cas system interference. In accordance with expression

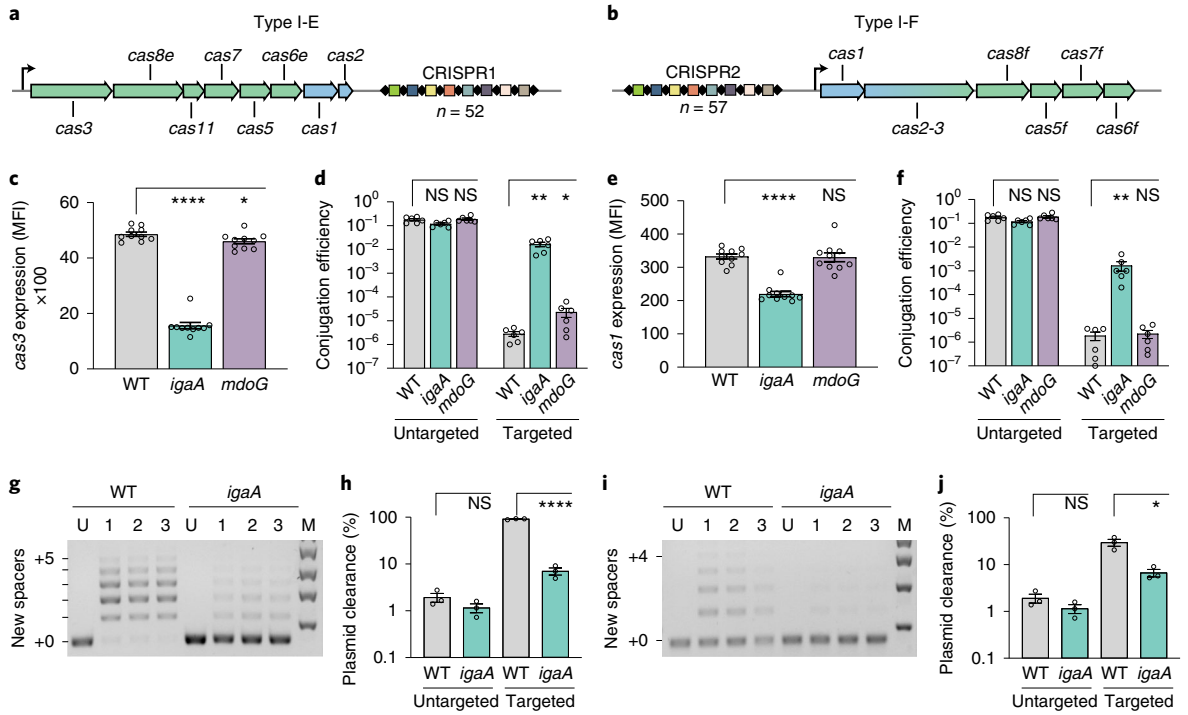

Fig. 4 | Induction of the Rcs pathway represses type I CRISPR–Cas activity and leads to decreased CRISPR adaptation and greater plasmid retention. **a**,**b**, Organization of the type I-E (**a**) and type I-F (**b**) CRISPR–Cas systems in *Serratia*, with the main *cas* promoters indicated by arrows. **c**, Expression of a *cas3* promoter–*eYFP* fusion (MFI; $n = 10$ biologically independent samples). **d**, Type I-E CRISPR–Cas interference measured through conjugation efficiency of a plasmid carrying a protospacer matching the endogenous CRISPR1 array (targeted) or a control (untargeted) ($n = 6$ biologically independent samples). **e**, Expression of a *cas1* promoter–*eYFP* fusion ($n = 10$ biologically independent samples). **f**, Type I-F CRISPR–Cas interference measured through conjugation efficiency of a plasmid carrying a protospacer matching the endogenous CRISPR2 array (targeted) or a control (untargeted) ($n = 6$ biologically independent samples). **g**, CRISPR adaptation as measured by expansion of the type I-E (CRISPR1) array after 2 d of passaging a priming-inducing plasmid ($n = 3$ biologically independent samples; M, molecular mass marker; U, untargeted control). **h**, Percentage of cells that cleared the type I-E priming (targeted) plasmid by day 2, compared with untargeted control ($n = 3$ biologically independent samples). **i**, CRISPR adaptation as measured by expansion of the type I-F (CRISPR2) array after 2 d of passaging a priming-inducing plasmid ($n = 3$ biologically independent samples). **j**, Percentage of cells that cleared the type I-F priming (targeted) plasmid by day 2, compared with untargeted control ($n = 3$ biologically independent samples). All bars represent the mean and error bars the s.e.m. To determine statistical significance, two-sided Student's *t*-tests were used for **c**, **e**, **h** and **j**, and Mann–Whitney *U*-tests for **d** and **f**. Detailed statistical testing can be found in the accompanying source data. $^{****}P < 0.0001$; $^{**}P < 0.01$; $^{*}P < 0.05$.

data, type I-E and I-F interference against plasmids carrying tetracycline resistance was decreased in the *igaA* mutant (10^3- and 10^4-fold, respectively) (Fig. 4d,f). Type I-E interference was also reduced—to a lesser extent—in the *mdoG* mutant (~10-fold, Fig. 4d), whereas no effect on type I-F targeting was detected (Fig. 4f), consistent with wild-type levels of *cas* operon expression in this strain (Fig. 4e). The reduced type I interference in these Rcs-activated strains was dependent on RcsB and RcsA, although deletion of *rcsA* had a weaker effect (Extended Data Fig. 3c). In summary, activation of the Rcs pathway represses both type I-E and I-F CRISPR–Cas expression and interference, which permits increased plasmid uptake and stability, thereby promoting the maintenance of antibiotic resistance genes.

The Rcs pathway represses type I spacer acquisition. We predicted that activation of the Rcs pathway would also repress CRISPR–Cas adaptation because the promoters of the type I operons (Fig. 4a,b, black arrows) control *cas* genes involved in both interference and spacer acquisition. New spacer integration into CRISPR arrays—the process of CRISPR adaptation—can be accelerated in type I systems by mismatches between the crRNA and their targets, in a process called priming[7,57,58]. To assess differences in adaptation between the wild-type and *igaA* mutant, we monitored CRISPR array expansion in response to plasmids that induce priming. In the wild-type, type I-E (CRISPR1) and type I-F (CRISPR2) arrays showed abundant acquisition of up to five new spacers, whereas minimal array expansion occurred in the *igaA* mutant (Fig. 4g,i). Acquisition of spacers through priming leads to interference and loss of the primed plasmid[58]. In agreement with the CRISPR-array expansion population profiles, faster plasmid clearance occurred in wild-type cells undergoing priming compared with the *igaA* mutant (Fig. 4h,j). Untargeted plasmids were stable, indicating that differences in plasmid loss were CRISPR dependent (Fig. 4h,j). In conclusion, Rcs pathway activation strongly inhibits the acquisition of new spacers, thus impairing priming-induced CRISPR–Cas targeting and enhancing plasmid retention.

The Rcs pathway confers innate cell-surface immunity against diverse phages. The finding that Rcs coordinately repressed CRISPR–Cas systems suggested that, under membrane stress, such as that induced by antibiotics[28,35], adaptive immunity is disfavoured. Indeed, these stress conditions might permit the acquisition and retention of plasmids that can be selected if they assist stress tolerance. However, under these scenarios, suppression of CRISPR–Cas immunity risks leaving bacteria prone to phage infection. We hypothesized that surface-based innate phage immunity is promoted by Rcs, because this pathway regulates various cell-surface properties[28]. Indeed, in the absence of CRISPR immunity (for example,

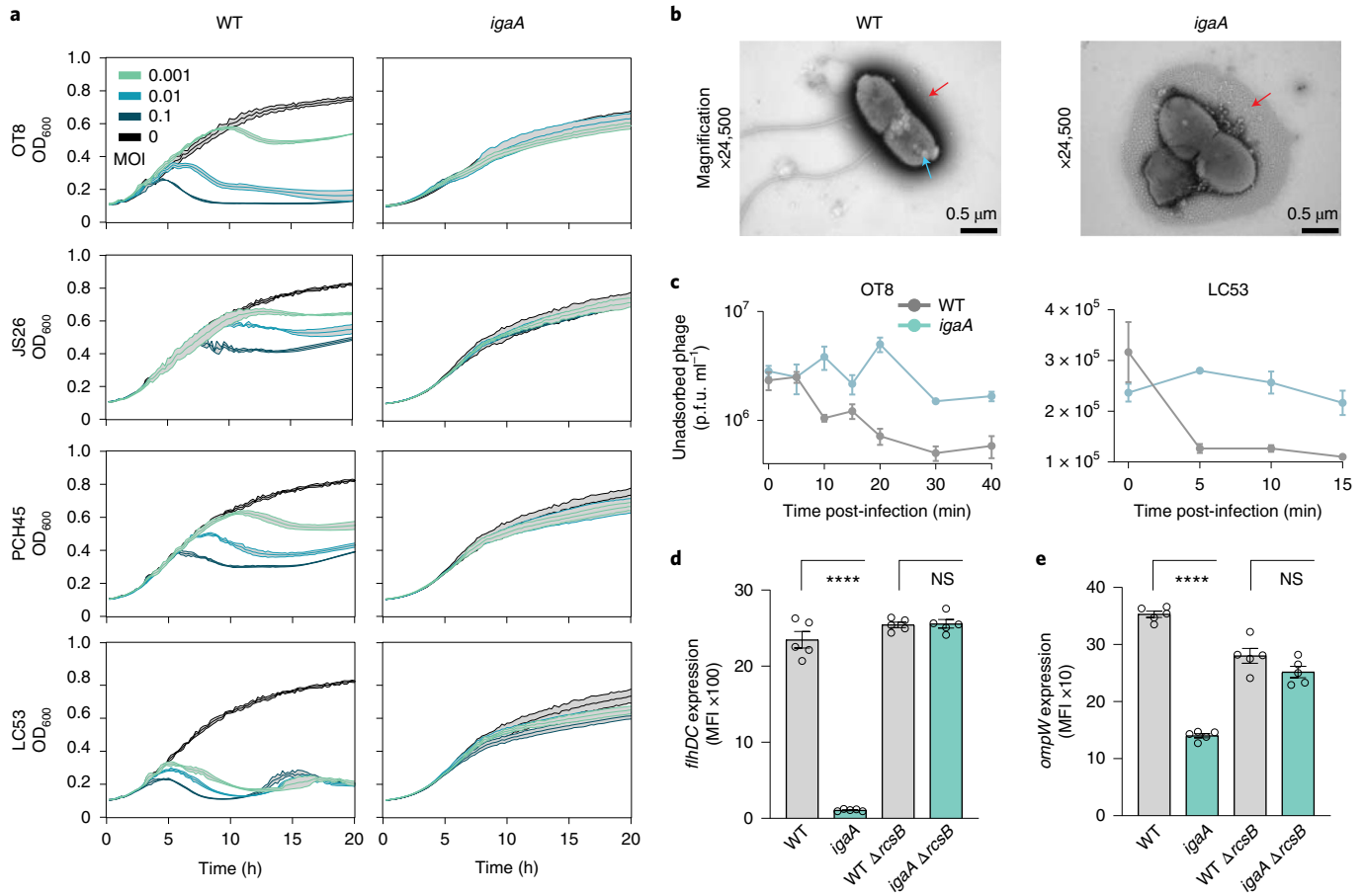

Fig. 5 | Mutations inducing the Rcs pathway confer innate immunity against phage infection. a, Infection by phages ϕOT8, JS26, PCH45 and LC53 is attenuated in mutants activating the Rcs pathway ($n = 3$ biologically independent samples; lines represent the mean ± s.d.). MOI, multiplicity of infection. **b**, Transmission electron microscopy of WT and *igaA*, with putative outer membrane vesicles (red arrows) and gas vesicles (blue arrows). Images represent independent biological samples ($n = 3$). **c**, Rcs activation in the *igaA* mutant blocks phage ϕOT8 and LC53 adsorption. Quantification of phage from the supernatant after infection ($n = 3$ independent biological samples; points shown are the mean and error bars represent the s.e.m.). **d**,**e**, Rcs-dependent repression of the flagella master regulators *flhDC* (**d**) and *ompW* (**e**) in the *igaA* strain ($n = 5$ biologically independent samples). All bars shown are the mean and error bars represent the s.e.m. For **d** and **e**, two-sided Student's *t*-tests were used to determine statistical significance. Detailed statistical testing can be found in the accompanying source data. ****$P < 0.0001$.

no phage-targeting spacers), the Rcs-activated (*igaA*) strain was resistant to four unrelated *Serratia* phages belonging to the *Siphoviridae* (ϕOT8 (ref. [59]) and JS26 (ref. [60])) and the *Myoviridae* (PCH45 (ref. [24]) and LC53) families (Fig. 5a and Extended Data Fig. 4a). The *mdoG* mutant also exhibited enhanced phage resistance, albeit to a lesser extent (Extended Data Fig. 4a,b).

We observed no flagella on *igaA* mutants when visualized by electron microscopy (Fig. 5b), and swimming was inhibited (*igaA*) or reduced (*mdoG*) in an RcsB-dependent manner (Extended Data Fig. 4c)—consistent with Rcs-mediated repression of the *flhDC* flagella master regulators in *E. coli* and *Salmonella enterica*[28]. As phages ϕOT8, JS26 and PCH45 require flagella for infection[59] (Malone et al., manuscript in preparation), this explains the surface-based immunity in the Rcs-activated strains against these phages (Fig. 5a and Extended Data Fig. 4a,b). In agreement, phage ϕOT8 failed to adsorb to the *igaA* mutant that lacked flagella (Fig. 5c), and deletion of *rcsB* restored phage susceptibility of the *igaA* and *mdoG* mutants (Extended Data Fig. 5a). To verify that motility and infection changes were due to receptor downregulation, we measured *flhDC* expression. A greater than 20-fold reduction in *flhDC* expression was observed in the Rcs-activated *igaA* mutant. The reduction was dependent on *rcsB* and to a lesser extent *rcsA* (Fig. 5d and Extended Data Fig. 6a), which is consistent with the partial restoration of swimming and phage infectivity on deletion of *rcsA* in the *igaA* mutant (Extended Data Figs. 4c and 5a). In accordance with motility and phage infection data, *rcsB*, but not *rcsA*, contributes to *flhDC* repression in the *mdoG* mutant (Extended Data Fig. 6a).

It is of interest that phage LC53, which uses OmpW as a receptor (Malone et al., manuscript in preparation), also failed to adsorb to the *igaA* mutant (Fig. 5c). We hypothesized that OmpW might be inaccessible due to capsule formation, which can confer phage resistance[61,62]. However, no capsule was visible in the *igaA* mutant (Fig. 5b), and expression of the only predicted capsule biosynthesis locus in *Serratia* was decreased in both *igaA* and *mdoG* mutants (Extended Data Fig. 2e). Although the function of the *wza* capsule biosynthesis operon in this strain of *Serratia* has not been described, its downregulation excludes a role for capsule formation in the observed phage resistance. Furthermore, outer membrane vesicle (OMV) production appeared elevated in the *igaA* mutant (Fig. 5b, red arrows), consistent with reported OMV stimulation in a *Serratia marcescens igaA* (*gumB*) mutant[63]. Cell stress is known to stimulate OMV production, which can serve as phage decoys[64,65]. However, OMVs made no detectable contribution to LC53 resistance because free phages did not decrease in the presence of OMVs produced

by the *igaA* mutant (Fig. 5c). Instead, we propose that Rcs activation confers LC53 resistance via receptor downregulation, because *ompW* promoter activity was reduced in the *igaA* mutant in an Rcs-dependent manner (Fig. 5e, and Extended Data Figs. 5b and 6b). The Rcs pathway may have a conserved role in *ompW* regulation, with a recent study demonstrating that *rcsB* mutation increased *ompW* in *Yersinia enterocolitica*[66].

The broad phage resistance offered by the *Serratia* Rcs system is consistent with multi-phage resistance observed recently in *E. coli* on *igaA* knockdown[67] or mutation[68]. Together, our data show that Rcs induction alters receptor and extracellular/cell-surface properties that limit phage adsorption and, thus, provide innate immunity against diverse phages. As phages fail to infect Rcs-activated strains, the requirement for CRISPR–Cas adaptation and interference becomes superfluous and is downregulated. The inverse control of surface versus adaptive immunity allows bacteria to acquire genetic material by conjugation in response to stress, while concomitantly protecting cells from detrimental phage infection (Fig. 6).

Discussion

In the present study, we have addressed the important question of how bacteria control their immune systems. Faced with a lack of high-throughput tools to identify regulators of bacterial gene expression, we developed a scalable functional genomics method that couples cell sorting with Tn insertion sequencing. We used this technology to assess *csm* gene expression for ~300,000 mutants and uncovered multiple pathways regulating CRISPR–Cas in *Serratia*. Many of these regulators are conserved in diverse bacteria, suggesting that they may control CRISPR–Cas systems more broadly—a hypothesis requiring testing across a range of bacteria.

The Rcs stress response phosphorelay was a major cascade that repressed both type III and type I CRISPR–Cas activity. Importantly, Rcs inversely controlled surface versus adaptive immunity by promoting cell-surface resistance, which reduced phage adsorption, while concomitantly repressing *cas* expression, interference and adaptation—thereby coordinating these two different defence strategies. Although cell-surface modifications can provide robust immunity against phages[69], they do not hamper the acquisition of foreign DNA through conjugation[70]. Thus, the Rcs response to stress provides broad-spectrum phage resistance while, through conjugation, allowing the uptake of genetic material that is potentially beneficial for stress adaptation. The enhanced acquisition of foreign DNA on CRISPR–Cas repression probably extends to transformation; however, *Serratia* is not naturally competent. Downregulation of CRISPR–Cas will presumably also increase the acquisition of non-beneficial elements, but these bacteria will be outcompeted by fitter community members. Rcs-mediated repression of CRISPR–Cas is not restricted to *Serratia* and might be a broader phenomenon. For example, in *Erwinia amylovora*, mutation of *rcsC* resulted in decreased type I-E expression[71], possibly due to activated RcsB accumulation (via acetyl phosphate[72]) in the absence of RcsC phosphatase activity[73,74].

The Rcs cascade can be activated by antimicrobials as well as alterations in LPS that interfere with the integrity of the periplasm and peptidoglycan[28]. Under stress conditions, downregulation of energetically costly structures such as flagella or multi-protein interference complexes may aid in re-allocating resources towards the stress response. Receptor downregulation not only confers phage resistance, but incurs only a transient cost when compared with permanent surface modifications, which carry fixed costs and reduce fitness[69,75]. Likewise, the CRISPR–Cas downregulation described in the present study enables acquisition of genes without potential costs of CRISPR–Cas inactivation. Past studies demonstrated that CRISPR–Cas mutants can arise on selection for antibiotic resistance genes or virulence genes delivered by conjugation or transformation in *Staphylococcus epidermidis*[76] and *Streptococcus pneumoniae*[77], respectively. Although costs and conditions that favour surface mutation over CRISPR–Cas immunity in response to phages has been analysed[75], further work is required on the effects of regulation on the costs and the different pressures from phages versus plasmids. Our results indicate that cellular stresses, through Rcs-mediated downregulation of CRISPR–Cas, can increase the ability of cells to both acquire and retain mobile elements, such as those encoding resistance determinants. Rcs activation also enhances intrinsic β-lactam resistance[78], as well as the formation of OMVs[79], which provide resistance to, and act as decoys against, antimicrobials and phages[64,80]. In addition, overexpression of *rcsB* upregulates the transcription of drug exporter genes[81].

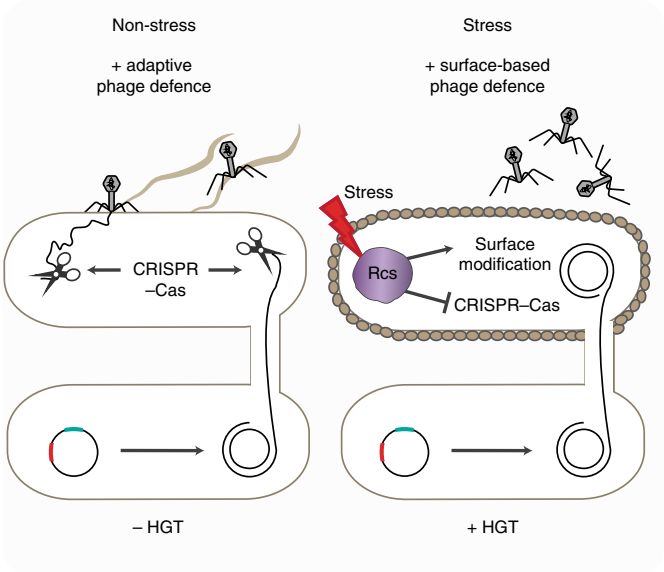

Fig. 6 | Proposed model of phage defence strategy and effects on HGT on Rcs phosphorelay activation. Under non-stress conditions, CRISPR–Cas inhibits HGT and provides adaptive immunity against phages. On cell stress, Rcs activation leads to enhanced innate phage resistance through cell-surface modifications and diminished CRISPR–Cas activity, which permits HGT and retention.

Phages are being pursued as a potential tool in the fight against drug-resistant bacteria[5], and co-therapies with antibiotics are being considered[82,83]. We hypothesize that perturbations that trigger Rcs and diminish CRISPR–Cas immunity may unintentionally promote surface-based phage resistance—potentially hampering the efficacy of phage therapies and promoting antimicrobial resistance. In addition, a recent study in *Salmonella enterica* demonstrated RcsB activation via a non-cognate histidine kinase—BarA of the carbon storage regulator (Csr/Rsm) system[84]—the homologue of which in *Serratia* (PigW) was also identified in our screen. This suggests the Rcs regulon can be fine-tuned in response to cues beyond its canonical role in outer-membrane stress. These are important considerations for the spread of resistance genes and treatment of drug-resistant bacteria. As Csr/Rsm regulatory pathways are widespread in Gram-negative and Gram-positive bacteria, and act post-transcriptionally, they warrant further examination into how they control CRISPR–Cas immunity.

Although Tn insertion sequencing[85,86] is powerful at addressing questions such as gene essentiality, genes involved in more complex phenotypes are not readily identified. Standard procedures for screening Tn libraries often rely on manual, highly complex or organism-specific methods[85,87]. In the present study, within hours, FACS facilitated rapid and reproducible enrichment of mutants conferring even subtle changes in gene expression. This technique will be widely adaptable to any strain that can harbour fluorescent

reporters and be mutagenized using transposons. The ease, robustness and customizability of this method demonstrate the potential of SorTn-seq for wide application to explore diverse biological questions in bacteria.

Methods

Bacterial and virus strain culturing. *Serratia* sp. ATCC 39006 (American Type Culture Collection catalogue no. 39006) strains were grown at 30 °C and *E. coli* at 37 °C in lysogeny broth (LB), with shaking at 200 r.p.m. LB containing 1.5% w:v agar (LBA) was used to grow strains on plates. The following supplements were added to the media when necessary: chloramphenicol (Cm, 25 μg ml^{-1}), kanamycin (Km, 50 μg ml^{-1}), tetracycline (Tc, 10 μg ml^{-1}), ampicillin (Amp, 100 μg ml^{-1}), isopropyl β-D-1-thiogalactopyranoside (IPTG, 100 μM) and 5-aminolaevulinic acid hydrochloride (ALA, 50 μg ml^{-1}). Plasmids were transformed into *E. coli* ST18 or DH5α via heat shock and moved into *Serratia* via conjugation using *E. coli* ST18 as the donor. All plasmids and strains were confirmed by Sanger sequencing. Bacteriophage stocks (ϕOT8, JS26, PCH45 and LC53) were propagated on *Serratia* (PCF396) grown in LB at 30 °C.

Mutant strain construction. Gene-deletion strains (Supplementary Table 4) were constructed using allelic exchange mutagenesis as previously described[56,88]. Briefly, ~500 bp upstream and downstream of the region to be deleted were PCR amplified separately. Primers (Supplementary Table 6) were designed with a region of overlap, so the 500-bp upstream and downstream regions would anneal and could be joined through overlap extension PCR, resulting in a ~1-kb product. This product was ligated into the *sacB*-containing suicide vector pPF1117 (ref. [60]) to create a gene-deletion construct (Supplementary Table 5) and transformed into *E. coli* ST18. In some cases, an antibiotic resistance cassette (Km^R) was introduced to generate a marked version of the deletion. Plasmids harbouring gene-deletion constructs were conjugated and subsequently integrated into the *Serratia* chromosome. Detection of a second homologous recombination event, resulting in the loss of the plasmid and deletion of the region of interest, were screened by plating on LBA supplemented with sucrose (10%, v:v). Sucrose-sensitive colonies were PCR screened for gene deletion and strains were confirmed by Sanger sequencing.

Tn mutant library construction. *E. coli* donor strain ST18 harbouring the Tn*5* transposon delivery plasmid pKRCPN2 was grown overnight in 5 ml of LB with ALA and Tc at 37 °C with shaking at 200 r.p.m. *Serratia* recipient strain PCF396 harbouring the P*csm* reporter plasmid pPF1334 was grown overnight in 5 ml of LB with Cm at 30 °C with shaking at 200 r.p.m. Cells were harvested via centrifugation at 8,000 *g* for 2 min. Cells were washed and resuspended in LB, the optical density at 600 nm (OD_{600}) was measured on a spectrophotometer, then each culture was standardized to an OD_{600} of 1. *E. coli* and *Serratia* were mixed together in equal volumes, then 30 (100-μl) aliquots were plated on 0.22-μm nitrocellulose filters (Millipore) atop LBA with ALA. Conjugation spots were incubated for 6 h at 30 °C, and filters were collected in 15 ml of LB to resuspend cells. Cells were inoculated into three flasks (2 l) containing 500 ml of LB (supplemented with Km and Cm) at a starting OD_{600} of 0.02 and grown at 30 °C with shaking (180 r.p.m.) for 24 h. This outgrowth selected for *Serratia* harbouring both the reporter plasmid and the Tn. After outgrowth, 15 ml of culture from each flask was pooled (45 ml in total) and centrifuged at 3,000 *g*. Cells were resuspended in LB to a final OD_{600} of 3 to generate the final Tn library. Aliquots (1 ml) of the library were mixed 1:1 with 50% glycerol and frozen in cryotubes at −80 °C for future use. Colony-forming unit measurements were taken pre-conjugation, post-conjugation and post-outgrowth to determine the proportions of *Serratia* and *E. coli* throughout the experiment.

FACS. Aliquots of 1 ml of frozen Tn mutant library were subcultured (starting $OD_{600} = 0.05$) into 30 ml of LB with Cm for reporter plasmid selection, Km for transposon selection and IPTG for mCherry induction. Cells were grown for 16 h to allow expression of the P*csm*–eYFP reporter. Before sorting, 1 ml of culture was removed for DNA extraction to serve as the input library. Cells were then diluted in 15 ml of phosphate-buffered saline (PBS, 1:30) and sorted using a FACSAria Fusion (BD Biosciences). Despite minimal spectral overlap between eYFP and mCherry, single stain controls (mCherry only—PCF396 + pPF1438; eYFP only—PCF396 + pPF1307; and unstained cells—PCF396) were used to establish a compensation matrix in the BD FACSDiva software (v.8, BD Biosciences). Cells were gated on forward scatter (FSC) and side scatter (SSC) parameters (area, height, width) as indicated in Supplementary Fig. 2a. The mCherry$^+$ cells were selected and sorted into three bins based on eYFP fluorescence levels. Gates high and low were each set at approximately 5% of the total, whereas the depleted gate was set at 90% (Supplementary Fig. 2a). Cells were sorted under 'purity' mode, and approximately 2.0×10^7 cells were sorted per experiment. Sorted cells were recovered in 0.2 ml of PBS. Outgrowth and sorting were performed in triplicate on different days, with each experiment yielding one low, one high, one depleted and one input fraction (total $n = 12$).

DNA extraction, library preparation and sequencing. Sorted cell fractions ($n = 9$) and input samples ($n = 3$) were centrifuged and DNA was extracted using the DNeasy Blood and Tissue Kit (QIAGEN) following the manufacturer's instructions. Sequencing libraries were constructed using the NEBNext Ultra II FS DNA Library Prep Kit for Illumina. The protocol was modified to have two rounds of PCR enrichment. Round one used customized PCR enrichment primers: PF3140, which binds the NEB adaptor, and PF3139, a biotinylated primer that binds within the Tn. Biotinylated products were captured using Dynabeads M-270 Streptavidin (Invitrogen) following the manufacturer's instructions, and beads were used as the template in the second-round PCR with a nested Tn primer PF3270 and an indexing primer (NEBNext Multiplex Oligos for Illumina). Library quality was assessed on an Agilent Bioanalyzer 2100 using a High Sensitivity DNA Kit. Libraries were further assessed through quantitative PCR (KAPA Library Quantification Kit, Universal, catalogue no. KK4824) using primers PF3124/PF3125 to determine molarity of fragments with Illumina P5/P7 ends (sequences required for flow-cell hybridization). Tn sequencing primer PF2926, along with PF3125, were used to determine the percentage of fragments containing true Tn sequences. Libraries were quantified using a Qubit fluorimeter and dsDNA HS Kit (Thermo Fisher Scientific) and diluted to 10 nM based on Qubit concentration and average fragment size. Libraries were then pooled with 10% PhiX control library and loaded at 1.5 pM (for low diversity) using a MiSeq Reagent Kit v.3 150 cycle kit for Illumina. Libraries were sequenced for 75 cycles (single ended) using custom sequencing primer PF2926 and Illumina Read 1 primer PF3441 (for PhiX library) at the Otago Genomics Facility (OGF). Sequencing with PF2926 generates a 12-nt transposon 'tag' to verify reads originating from Tn junctions.

Data analysis. Samples were de-multiplexed based on index sequence by OGF using standard Illumina software. FASTQ files were trimmed from the 3′-end to 50 nt using PRINSEQ lite[89] and mapped to reference sequences using the Bio-Tradis pipeline (https://github.com/sanger-pathogens/Bio-Tradis)[90]. The following parameters were used to run the bacteria_tradis script: '-smalt -smalt_k 10 -smalt_s 1 -smalt_y 0.92 -mm 2 -v -f filelist.txt -t TATAAGAGACAG -r laca. fasta', where -smalt_ commands specify mapping parameters, -t specifies the transposon tag sequence, -r specifies the reference sequence, -f indicates the files to be processed and -mm indicates the number of mismatches allowed in the Tn tag. In summary, only reads containing the Tn tag (minimum 10/12 identity) and 92% identity to the reference sequence were considered. Plot files (.insert_site_plot), which tabulate the number of reads at each nucleotide position in the reference sequence (plus and minus strands), were generated by the bacteria_tradis script. Subsequent analysis was performed in R using customized scripts (https://github.com/JacksonLab/SorTn-seq). Plot files were used to generate a table of unique Tn insertion sites (for each sample). Feature enrichment was determined using differential expression analysis (exact methods—classic) of unique insertions in edgeR[29]. The depleted samples served as the control group, against which low and high samples were compared. Only features containing more than two unique insertions in all depleted samples were included, allowing enrichment analysis of 3,475 of 4,035 National Center for Biotechnology Information (NCBI)-annotated features (~86%) and 1,105 of 2,933 (~39%) of the manually annotated intergenic regions. Using this approach, and our estimated Tn density of 1 insertion per 17 nt (Fig. 1e), we estimated that even the smallest NCBI-annotated features (for example, transfer RNAs, ~70 nt) had adequate saturation for analysis (~4 insertions), excluding feature essentiality/fitness effects. We then considered features with an adjusted $P < 0.05$ (Benjamini–Hochberg false discovery rate (FDR) correction) and a $\log_2$(fold-change (FC)) > 0.5 as potential regulators.

Expression analysis via flow cytometry. Cells were grown for 20 h in 1 ml of LB with appropriate supplements in a 96-deep well plate (Labcon) at 30 °C with shaking at 1,200 r.p.m. in an IncuMix incubator shaker (Select BioProducts). Cells were diluted in PBS (1:1,000 or adjusted when necessary) before sample measurement. Fluorescent reporter expression was measured using a LSRFortessa flow cytometer (BD Biosciences). A threshold was applied for FSC and SSC to detect bacterial cells. The eYFP was excited using a blue laser (488 nm) and detected with a 530/30 nm bandpass filter; mCherry was excited using a yellow–green laser (561 nm) and detected with a 610/20 nm bandpass filter; 20,000 events were recorded per sample using the BD FACSDiva software (v.8, BD Biosciences). Subsequent analysis was performed using FlowJo software v.10 (BD Biosciences). Cells were gated on FSC-A/SSC-A and SSC-A/SSC-H, then positive mCherry expression, to determine the eYFP median fluorescence intensity (MFI) of cell populations. A minimum of five biological replicates per strain were used for each experiment, and data plotted as the mean ± s.e.m. Statistical significance was determined using a two-tailed Student's *t*-test (with Welch's correction where appropriate) of wild-type versus mutant.

Plasmid interference conjugation efficiency assays. *E. coli* ST18 were used as donors for the conjugation of type I-E-targeted (pPF724), type I-F-targeted (pPF722), type I-untargeted control (pPF719), type III-A-targeted (pPF1043) or type III-A-untargeted control (pPF781) plasmids. Plasmids pPF724, pPF722 and pPF1043 each contain a protospacer targeted by spacer 1 from CRISPR1 (type I-E), CRISPR2 (type I-F) or CRISPR3 (type III-A), respectively. Recipient strains were wild-type (PCF396), *mdoG* (PCF625) *igaA* (PCF692), and Δ*rcsA* (PCF817-819) or Δ*rcsB* (PCF695-697) derivatives. Strains were grown overnight

in LB with appropriate antibiotics, washed twice with LB and adjusted to an OD_{60} of 1. Donors and recipients were mixed in a 1:1 ratio, and 20 µl was spotted on to 0.22-µm nitrocellulose filters (Millipore) atop LBA with ALA, and incubated for 24 h at 30 °C. Next, the filters were added to 500 µl of PBS, the bacteria were resuspended and dilution series were plated on to LBA to enumerate recipients, or LBA with the addition of antibiotics for transconjugant counts. As targeting by type III systems is transcription dependent, 0.02% arabinose (v:v) was added to the LBA for protospacer transcription during transconjugant selection. During initial conjugation, 0.2% glucose (v:v) was added to LBA to repress targeting. Conjugation efficiency was expressed as the total number of transconjugants per recipient. Each condition was performed either three or six times with data plotted as the mean ± s.e.m. Statistical significance was determined via the Mann–Whitney *U*-test of wild-type versus mutant.

CRISPR-primed adaptation assay. CRISPR adaptation assays were performed as previously described[56]. Plasmids pPF953 (unprimed control), pPF1233 (type I-E-priming plasmid) and pPF1236 (type I-F-priming plasmid) were conjugated into strains PCF396 and PCF692. Strains harbouring plasmids were grown for 24 h in 5 ml of LB plus Tc selection at 30 °C, with shaking at 200 r.p.m. These 'day 0' cultures were then used to inoculate (1:500 dilution) 5 ml of fresh LB supplemented with IPTG without selection and incubated again. This process was repeated for 2 d. Aliquots of culture from each day were mixed 1:1 with 50% glycerol and frozen at −80 °C for future use. CRISPR array expansion (indicative of adaptation) was assessed via PCR with primers PF633/PF2177 for type I-E (CRISPR1) and PF1888/PF1990 for type I-F (CRISPR2). Each condition was performed in triplicate.

Primed plasmid clearance assays. Plasmid loss was measured as previously described[60]. Cells from the adaptation assay were analysed using a LSRFortessa flow cytometer (BD Biosciences) as described in Expression analysis via flow cytometry. Analysis was performed using FlowJo software v.10 (BD Biosciences). Cells were gated on SSC-A/SSC-H and SSC-A/FSC-A, then bifurcated (using BifurGate) into $mCherry^+$ and $mCherry^-$ populations (Supplementary Fig. 2b). The ratio of $mCherry^-$ cells to total cells indicates what proportion of cells has cleared the plasmid. Plasmid clearance (%) is plotted as the mean ± s.e.m. ($n = 3$ biologically independent samples). Statistical significance was determined using a two-tailed Student's *t*-test of wild-type versus the *igaA* mutant.

Phage resistance infection growth curves. *Serratia* stationary phase cultures were normalized to a starting OD_{600} of 0.05 in 180 µl of LB in a 96-well plate. Of the phage lysate (10-fold serially diluted), 20 µl was added to each well to produce the desired multiplicity of infection (MOI). Alternatively, 20 µl of phage buffer was added for the no-phage control. The 96-well plate was incubated in a Varioskan Flash plate reader (Thermo Fisher Scientific) at 30 °C with shaking at 300 r.p.m. and OD_{600} measurements taken at 12-min increments for 21–24 h. Each condition was performed in triplicate with data plotted as the mean ± s.d.

Phage plaquing assays. A 4-ml LBA overlay (0.35% w:v agar) containing 100 µl of bacterial culture was poured over an LBA plate. Serial 10-fold dilutions of phage stocks (~10^{11} plaque-forming units (p.f.u.) ml^{-1}) were spotted (20 µl) on to the overlay surface and incubated overnight at 30 °C. All conditions were performed in triplicate.

Phage adsorption assays. *Serratia* stationary phase cultures were diluted to a starting OD_{600} of 0.05 in 10 ml of LB and grown at 30 °C with shaking at 200 r.p.m. until reaching an OD_{600} of 0.3. Cells were infected with ϕOT8 or LC53 at an MOI of 0.01. Samples were removed at the following time points post-infection: 0, 5, 10, 15, 20, 30 and 40 min. At each time point, 200 µl of infected culture was removed and centrifuged for 1 min at 13,000 *g* to separate cells. Of the supernatant, 100 µl was then transferred to 96-well plates where serial 10-fold dilutions were made. A 4-ml LBA overlay (0.35% w:v agar) containing 100 µl of wild-type (PCF396) culture was poured over an LBA plate. Spots (20 µl) were plated on to the overlay surface and incubated overnight at 30 °C. The number of plaques were counted to calculate p.f.u. ml^{-1}. All conditions were repeated in triplicate and plotted as the mean ± s.e.m.

Electron microscopy. Transmission electron microscopy was performed as previously described[24]. Briefly, 10 µl of stationary-phase liquid culture was loaded on to plasma-glowed, carbon-coated, 300-mesh copper grids. After 1 min, the excess culture was removed by blotting with filter paper; 10 µl of phosphotungstic acid (1%, w:v, pH 7.2) was then applied to the grid for negative staining and blotted off immediately. The grids were viewed in a Philips CM100 BioTWIN transmission electron microscope (Philips/FEI Corporation) and images captured using a MegaView lll digital camera (Soft Imaging System GmbH). Three independent biological samples were prepared and imaged for each strain.

Swimming motility assays. Swim plates were prepared using tryptone swarm agar (10 g of tryptone, 5 g of NaCl, 3 g of agar per litre). Plates were inoculated with 2 µl of exponential phase cultures by stabbing through the agar with a pipette tip, and then incubated for 24 h at 30 °C.

β-Galactosidase expression assays. Expression of *lacZ* reporters was measured using the fluorogenic substrate (4-methylumbelliferyl-β-D-galactoside (MUG)) as previously described[56,91,92]. Briefly, strains with integrated P*csm-lacZ* reporters (PCF802, PCF804, PCF805), no-reporter controls (PCF396, PCF625, PCF692) and a no-cell control were grown for 20 h in 1 ml of LB supplemented with Tc (where appropriate) in a 96-deep well plate (Labcon) at 30 °C with shaking at 1,200 r.p.m. in an IncuMix incubator shaker (Select BioProducts). The OD_{600} was measured, cells were lysed and then treated with the MUG reagent. Fluorescence was measured in a Varioskan Flash Multimode Reader (Thermo Fisher Scientific) and relative fluorescent units per second (r.f.u. s^{-1}) were calculated using the linear increase in fluorescence. Fluorescence rates were normalized by the OD_{600} of the sample and are displayed as r.f.u. s^{-1} per OD_{600}—in arbitrary units. All conditions were performed six times and plotted as the mean ± s.e.m.

Reporting Summary. Further information on research design is available in the Nature Research Reporting Summary linked to this article.

Data availability

Additional data that support the findings of the present study are available from the corresponding author upon request. Sequencing data are available in the Sequence Read Archive under BioProject no. PRJNA601789. The annotated genome of *Serratia* sp. ATCC 39006—LacA is available through the NCBI (reference sequence NZ_CP025085.1) (https://www.ncbi.nlm.nih.gov/nuccore/NZ_CP025085.1). Source data are provided with this paper.

Code availability

Custom R scripts (SorTnSeq.R and SorTnSeq_Statistics.R) and files required for data processing (serratia_master_features_table.xlsx) are available on GitHub (https://github.com/JacksonLab/SorTn-seq).

Received: 30 August 2020; Accepted: 23 October 2020;
Published online: 4 January 2021

References

1. Hampton, H. G., Watson, B. N. J. & Fineran, P. C. The arms race between bacteria and their phage foes. *Nature* **577**, 327–336 (2020).
2. Hille, F. et al. The biology of CRISPR–Cas: backward and forward. *Cell* **172**, 1239–1259 (2018).
3. Partridge, S. R., Kwong, S. M., Firth, N. & Jensen, S. O. Mobile genetic elements associated with antimicrobial resistance. *Clin. Microbiol. Rev.* **31**, https://doi.org/10.1128/CMR.00088-17 (2018).
4. Willyard, C. The drug-resistant bacteria that pose the greatest health threats. *Nature* **543**, 15–15 (2017).
5. Kortright, K. E., Chan, B. K., Koff, J. L. & Turner, P. E. Phage therapy: a renewed approach to combat antibiotic-resistant bacteria. *Cell Host Microbe* **25**, 219–232 (2019).
6. Bernheim, A. & Sorek, R. The pan-immune system of bacteria: antiviral defence as a community resource. *Nat. Rev. Microbiol.* **18**, 113–119 (2020).
7. Jackson, S. A. et al. CRISPR–Cas: adapting to change. *Science* **356**, https://doi.org/10.1126/science.aal5056 (2017).
8. Makarova, K. S. et al. Evolutionary classification of CRISPR–Cas systems: a burst of class 2 and derived variants. *Nat. Rev. Microbiol.* https://doi.org/10.1038/s41579-019-0299-x (2019).
9. Nicholson, T. J. et al. Bioinformatic evidence of widespread priming in type I and II CRISPR–Cas systems. *RNA Biol.* **16**, 566–576 (2019).
10. Silas, S. et al. Type III CRISPR-Cas systems can provide redundancy to counteract viral escape from type I systems. *eLife* **6**, https://doi.org/10.7554/eLife.27601 (2017).
11. Deng, L., Garrett, R. A., Shah, S. A., Peng, X. & She, Q. A novel interference mechanism by a type IIIB CRISPR-Cmr module in *Sulfolobus*. *Mol. Microbiol.* **87**, 1088–1099 (2013).
12. Elmore, J. R. et al. Bipartite recognition of target RNAs activates DNA cleavage by the type III-B CRISPR–Cas system. *Genes Dev.* **30**, 447–459 (2016).
13. Tamulaitis, G., Venclovas, C. & Siksnys, V. Type III CRISPR–Cas immunity: major differences brushed aside. *Trends Microbiol.* **25**, 49–61 (2017).
14. Kazlauskiene, M., Kostiuk, G., Venclovas, C., Tamulaitis, G. & Siksnys, V. A cyclic oligonucleotide signaling pathway in type III CRISPR–Cas systems. *Science* **357**, 605–609 (2017).
15. Niewoehner, O. et al. Type III CRISPR–Cas systems produce cyclic oligoadenylate second messengers. *Nature* **548**, 543–548 (2017).
16. McMahon, S. A. et al. Structure and mechanism of a type III CRISPR defence DNA nuclease activated by cyclic oligoadenylate. *Nat. Commun.* **11**, 500 (2020).
17. Vercoe, R. B. et al. Cytotoxic chromosomal targeting by CRISPR/Cas systems can reshape bacterial genomes and expel or remodel pathogenicity islands. *PLoS Genet.* **9**, e1003454 (2013).

18. Stern, A., Keren, L., Wurtzel, O., Amitai, G. & Sorek, R. Self-targeting by CRISPR: gene regulation or autoimmunity? *Trends Genet.* **26**, 335–340 (2010).
19. Vale, P. F. et al. Costs of CRISPR–Cas-mediated resistance in *Streptococcus thermophilus*. *Proc. Biol. Sci.* **282**, 20151270 (2015).
20. Weissman, J. L., Stoltzfus, A., Westra, E. R. & Johnson, P. L. F. Avoidance of self during CRISPR immunization. *Trends Microbiol.* **28**, 543–553 (2020).
21. Patterson, A. G., Yevstigneyeva, M. S. & Fineran, P. C. Regulation of CRISPR–Cas adaptive immune systems. *Curr. Opin. Microbiol.* **37**, 1–7 (2017).
22. Smith, L. M., Rey Campa, A. & Fineran, P. C. in *CRISPR–Cas systems* (eds Marraffini, L. A. et al.) (ASM Press, 2021).
23. Pyenson, N. C., Gayvert, K., Varble, A., Elemento, O. & Marraffini, L. A. Broad targeting specificity during bacterial type III CRISPR–Cas immunity constrains viral escape. *Cell Host Microbe* **22**, 343–353 e343 (2017).
24. Malone, L. M. et al. A jumbo phage that forms a nucleus-like structure evades CRISPR–Cas DNA targeting but is vulnerable to type III RNA-based immunity. *Nat. Microbiol.* **5**, 48–55 (2020).
25. Shinkai, A. et al. Transcription activation mediated by a cyclic AMP receptor protein from *Thermus thermophilus* HB8. *J. Bacteriol.* **189**, 3891–3901 (2007).
26. Bernal-Bernal, D. et al. Multifactorial control of the expression of a CRISPR–Cas system by an extracytoplasmic function sigma/anti-sigma pair and a global regulatory complex. *Nucleic Acids Res.* **46**, 6726–6745 (2018).
27. Agari, Y. et al. Transcription profile of *Thermus thermophilus* CRISPR systems after phage infection. *J. Mol. Biol.* **395**, 270–281 (2010).
28. Wall, E., Majdalani, N. & Gottesman, S. The complex Rcs regulatory cascade. *Annu. Rev. Microbiol.* **72**, 111–139 (2018).
29. Robinson, M. D., McCarthy, D. J. & Smyth, G. K. edgeR: a Bioconductor package for differential expression analysis of digital gene expression data. *Bioinformatics* **26**, 139–140 (2010).
30. Gottesman, S., Trisler, P. & Torres-Cabassa, A. Regulation of capsular polysaccharide synthesis in *Escherichia coli* K-12: characterization of three regulatory genes. *J. Bacteriol.* **162**, 1111–1119 (1985).
31. Hussein, N. A., Cho, S. H., Laloux, G., Siam, R. & Collet, J. F. Distinct domains of *Escherichia coli* IgaA connect envelope stress sensing and down-regulation of the Rcs phosphorelay across subcellular compartments. *PLoS Genet.* **14**, e1007398 (2018).
32. Cho, S. H. et al. Detecting envelope stress by monitoring beta-barrel assembly. *Cell* **159**, 1652–1664 (2014).
33. Castanie-Cornet, M. P., Cam, K. & Jacq, A. RcsF is an outer membrane lipoprotein involved in the RcsCDB phosphorelay signaling pathway in *Escherichia coli*. *J. Bacteriol.* **188**, 4264–4270 (2006).
34. Wall, E. A., Majdalani, N. & Gottesman, S. IgaA negatively regulates the Rcs phosphorelay via contact with the RcsD phosphotransfer protein. *PLoS Genet.* **16**, e1008610 (2020).
35. Guo, X. P. & Sun, Y. C. New insights into the non-orthodox two component Rcs phosphorelay system. *Front. Microbiol.* **8**, 2014 (2017).
36. Stout, V., Torres-Cabassa, A., Maurizi, M. R., Gutnick, D. & Gottesman, S. RcsA, an unstable positive regulator of capsular polysaccharide synthesis. *J. Bacteriol.* **173**, 1738–1747 (1991).
37. Gottesman, S. & Stout, V. Regulation of capsular polysaccharide synthesis in *Escherichia coli* K12. *Mol. Microbiol.* **5**, 1599–1606 (1991).
38. Sledjeski, D. & Gottesman, S. A small RNA acts as an antisilencer of the H-NS-silenced rcsA gene of *Escherichia coli*. *Proc. Natl Acad. Sci. USA* **92**, 2003–2007 (1995).
39. Ebel, W. & Trempy, J. E. *Escherichia coli* RcsA, a positive activator of colanic acid capsular polysaccharide synthesis, functions to activate its own expression. *J. Bacteriol.* **181**, 577–584 (1999).
40. Majdalani, N., Chen, S., Murrow, J., St John, K. & Gottesman, S. Regulation of RpoS by a novel small RNA: the characterization of RprA. *Mol. Microbiol.* **39**, 1382–1394 (2001).
41. Majdalani, N., Hernandez, D. & Gottesman, S. Regulation and mode of action of the second small RNA activator of RpoS translation, RprA. *Mol. Microbiol.* **46**, 813–826 (2002).
42. Bohin, J. P. Osmoregulated periplasmic glucans in Proteobacteria. *FEMS Microbiol. Lett.* **186**, 11–19 (2000).
43. Bontemps-Gallo, S., Bohin, J. & Lacroix, J. Osmoregulated periplasmic glucans. *EcoSal Plus* https://doi.org/10.1128/ecosalplus.ESP-0001-2017 (2017).
44. Bontemps-Gallo, S. & Lacroix, J. M. New insights into the biological role of the osmoregulated periplasmic glucans in pathogenic and symbiotic bacteria. *Environ. Microbiol. Rep.* **7**, 690–697 (2015).
45. Ebel, W., Vaughn, G. J., Peters, H. K.III. & Trempy, J. E. Inactivation of mdoH leads to increased expression of colanic acid capsular polysaccharide in *Escherichia coli*. *J. Bacteriol.* **179**, 6858–6861 (1997).
46. Bontemps-Gallo, S. et al. Concentration of osmoregulated periplasmic glucans (OPGs) modulates the activation level of the RcsCD RcsB phosphorelay in the phytopathogen bacteria *Dickeya dadantii*. *Environ. Microbiol.* **15**, 881–894 (2013).
47. Girgis, H. S., Liu, Y., Ryu, W. S. & Tavazoie, S. A comprehensive genetic characterization of bacterial motility. *PLoS Genet.* **3**, 1644–1660 (2007).
48. Madec, E., Bontemps-Gallo, S. & Lacroix, J. M. Increased phosphorylation of the RcsB regulator of the RcsCDB phosphorelay in strains of *Dickeya dadantii* devoid of osmoregulated periplasmic glucans revealed by Phos-tag gel analysis. *Microbiology* **160**, 2763–2770 (2014).
49. Bouchart, F. et al. The virulence of a *Dickeya dadantii* 3937 mutant devoid of osmoregulated periplasmic glucans is restored by inactivation of the RcsCD–RcsB phosphorelay. *J. Bacteriol.* **192**, 3484–3490 (2010).
50. Konovalova, A., Perlman, D. H., Cowles, C. E. & Silhavy, T. J. Transmembrane domain of surface-exposed outer membrane lipoprotein RcsF is threaded through the lumen of beta-barrel proteins. *Proc. Natl Acad. Sci. USA* **111**, E4350–E4358 (2014).
51. Rigel, N. W. & Silhavy, T. J. Making a beta-barrel: assembly of outer membrane proteins in Gram-negative bacteria. *Curr. Opin. Microbiol.* **15**, 189–193 (2012).
52. Konovalova, A., Mitchell, A. M. & Silhavy, T. J. A lipoprotein/beta-barrel complex monitors lipopolysaccharide integrity transducing information across the outer membrane. *eLife* **5**, https://doi.org/10.7554/eLife.15276 (2016).
53. Kalynych, S., Morona, R. & Cygler, M. Progress in understanding the assembly process of bacterial O-antigen. *FEMS Microbiol. Rev.* **38**, 1048–1065 (2014).
54. Ren, G., Wang, Z., Li, Y., Hu, X. & Wang, X. Effects of lipopolysaccharide core sugar deficiency on colanic acid biosynthesis in *Escherichia coli*. *J. Bacteriol.* **198**, 1576–1584 (2016).
55. Wang, C. et al. Colanic acid biosynthesis in *Escherichia coli* is dependent on lipopolysaccharide structure and glucose availability. *Microbiol. Res.* **239**, 126527 (2020).
56. Patterson, A. G. et al. Quorum sensing controls adaptive immunity through the regulation of multiple CRISPR–Cas systems. *Mol. Cell* **64**, 1102–1108 (2016).
57. Datsenko, K. A. et al. Molecular memory of prior infections activates the CRISPR/Cas adaptive bacterial immunity system. *Nat. Commun.* **3**, 945 (2012).
58. Swarts, D. C., Mosterd, C., van Passel, M. W. & Brouns, S. J. CRISPR interference directs strand specific spacer acquisition. *PLoS ONE* **7**, e35888 (2012).
59. Evans, T. J. et al. Characterization of a broad-host-range flagellum-dependent phage that mediates high-efficiency generalized transduction in, and between, *Serratia* and *Pantoea*. *Microbiology* **156**, 240–247 (2010).
60. Jackson, S. A., Birkholz, N., Malone, L. M. & Fineran, P. C. Imprecise spacer acquisition generates CRISPR–Cas immune diversity through primed adaptation. *Cell Host Microbe* **25**, 250–260 e254 (2019).
61. Rendueles, O., Garcia-Garcera, M., Neron, B., Touchon, M. & Rocha, E. P. C. Abundance and co-occurrence of extracellular capsules increase environmental breadth: implications for the emergence of pathogens. *PLoS Pathog.* **13**, e1006525 (2017).
62. Paynter, M. J. & Bungay, H. R. III. Capsular protection against virulent coliphage infection. *Biotechnol. Bioeng.* **12**, 341–346 (1970).
63. Stella, N. A. et al. An IgaA/UmoB family protein from *Serratia marcescens* regulates motility, capsular polysaccharide biosynthesis, and secondary metabolite production. *Appl. Environ. Microbiol.* **84**, https://doi.org/10.1128/AEM.02575-17 (2018).
64. Schwechheimer, C. & Kuehn, M. J. Outer-membrane vesicles from Gram-negative bacteria: biogenesis and functions. *Nat. Rev. Microbiol.* **13**, 605–619 (2015).
65. Dineshkumar, K. et al. Bacterial bug-out bags: outer membrane vesicles and their proteins and functions. *J. Microbiol.* https://doi.org/10.1007/s12275-020-0026-3 (2020).
66. Meng, J., Bai, J. & Chen, J. Transcriptomic analysis reveals the role of RcsB in suppressing bacterial chemotaxis, flagellar assembly and infection in *Yersinia enterocolitica*. *Curr. Genet.* https://doi.org/10.1007/s00294-020-01083-x (2020).
67. Rousset, F. et al. Genome-wide CRISPR-dCas9 screens in *E. coli* identify essential genes and phage host factors. *PLoS Genet.* **14**, e1007749 (2018).
68. Mutalik, V. K. et al. High-throughput mapping of the phage resistance landscape in *E. coli*. *PLoS Biol.* **18**, e3000877 (2020).
69. van Houte, S., Buckling, A. & Westra, E. R. Evolutionary ecology of prokaryotic immune mechanisms. *Microbiol. Mol. Biol. Rev.* **80**, 745–763 (2016).
70. Perez-Mendoza, D. & de la Cruz, F. *Escherichia coli* genes affecting recipient ability in plasmid conjugation: are there any? *BMC Genomics* **10**, 71 (2009).
71. Wang, D. et al. Genome-wide identification of genes regulated by the Rcs phosphorelay system in *Erwinia amylovora*. *Mol. Plant Microbe Interact.* **25**, 6–17 (2012).
72. Fredericks, C. E., Shibata, S., Aizawa, S., Reimann, S. A. & Wolfe, A. J. Acetyl phosphate-sensitive regulation of flagellar biogenesis and capsular biosynthesis depends on the Rcs phosphorelay. *Mol. Microbiol.* **61**, 734–747 (2006).
73. Ancona, V., Chatnaparat, T. & Zhao, Y. Conserved aspartate and lysine residues of RcsB are required for amylovoran biosynthesis, virulence, and DNA binding in *Erwinia amylovora*. *Mol. Genet. Genomics* **290**, 1265–1276 (2015).

74. Garcia-Calderon, C. B., Garcia-Quintanilla, M., Casadesus, J. & Ramos-Morales, F. Virulence attenuation in *Salmonella enterica rcsC* mutants with constitutive activation of the Rcs system. *Microbiology* **151**, 579–588 (2005).
75. Westra, E. R. et al. Parasite exposure drives selective evolution of constitutive versus inducible defense. *Curr. Biol.* **25**, 1043–1049 (2015).
76. Jiang, W. et al. Dealing with the evolutionary downside of CRISPR immunity: bacteria and beneficial plasmids. *PLoS Genet.* **9**, e1003844 (2013).
77. Bikard, D., Hatoum-Aslan, A., Mucida, D. & Marraffini, L. A. CRISPR interference can prevent natural transformation and virulence acquisition during in vivo bacterial infection. *Cell Host Microbe* **12**, 177–186 (2012).
78. Laubacher, M. E. & Ades, S. E. The Rcs phosphorelay is a cell envelope stress response activated by peptidoglycan stress and contributes to intrinsic antibiotic resistance. *J. Bacteriol.* **190**, 2065–2074 (2008).
79. McMahon, K. J., Castelli, M. E., Garcia Vescovi, E. & Feldman, M. F. Biogenesis of outer membrane vesicles in *Serratia marcescens* is thermoregulated and can be induced by activation of the Rcs phosphorelay system. *J. Bacteriol.* **194**, 3241–3249 (2012).
80. Manning, A. J. & Kuehn, M. J. Contribution of bacterial outer membrane vesicles to innate bacterial defense. *BMC Microbiol.* **11**, 258 (2011).
81. Hirakawa, H., Nishino, K., Hirata, T. & Yamaguchi, A. Comprehensive studies of drug resistance mediated by overexpression of response regulators of two-component signal transduction systems in *Escherichia coli*. *J. Bacteriol.* **185**, 1851–1856 (2003).
82. Abedon, S. T. Phage-antibiotic combination treatments: antagonistic impacts of antibiotics on the pharmacodynamics of phage therapy? *Antibiotics* **8**, https://doi.org/10.3390/antibiotics8040182 (2019).
83. Hesse, S. & Adhya, S. Phage therapy in the twenty-first century: facing the decline of the antibiotic era; is it finally time for the age of the phage? *Annu. Rev. Microbiol.* **73**, 155–174 (2019).
84. Salvail, H. & Groisman, E. A. The phosphorelay BarA/SirA activates the non-cognate regulator RcsB in *Salmonella enterica*. *PLoS Genet.* **16**, e1008722 (2020).
85. Cain, A. K. et al. A decade of advances in transposon-insertion sequencing. *Nat. Rev. Genet.* https://doi.org/10.1038/s41576-020-0244-x (2020).
86. van Opijnen, T. & Levin, H. L. Transposon insertion sequencing, a global measure of gene function. *Annu. Rev. Genet.* https://doi.org/10.1146/annurev-genet-112618-043838 (2020).
87. Kwon, Y. M., Ricke, S. C. & Mandal, R. K. Transposon sequencing: methods and expanding applications. *Appl. Microbiol. Biotechnol.* **100**, 31–43 (2016).
88. Richter, C. et al. Priming in the type I-F CRISPR–Cas system triggers strand-independent spacer acquisition, bi-directionally from the primed protospacer. *Nucleic Acids Res.* **42**, 8516–8526 (2014).
89. Schmieder, R. & Edwards, R. Quality control and preprocessing of metagenomic datasets. *Bioinformatics* **27**, 863–864 (2011).
90. Barquist, L. et al. The TraDIS toolkit: sequencing and analysis for dense transposon mutant libraries. *Bioinformatics* **32**, 1109–1111 (2016).
91. Patterson, A. G., Chang, J. T., Taylor, C. & Fineran, P. C. Regulation of the type I-F CRISPR–Cas system by CRP-cAMP and GalM controls spacer acquisition and interference. *Nucleic Acids Res.* **43**, 6038–6048 (2015).
92. Ramsay, J. High-throughput β-galactosidase and β-glucuronidase assays using fluorogenic substrates. *Bio-protocol* **3**, e827 (2013).
93. Ashburner, M. et al. Gene Ontology: tool for the unification of biology. *Nat. Genet.* **25**, 25–29 (2000).
94. The Gene Ontology Consortium. The gene ontology resource: 20 years and still GOing strong. *Nucleic Acids Res.* **47**, D330–D338 (2019).

Acknowledgements

This work was supported by the Marsden Fund from the Royal Society of New Zealand (to P.C.F. and P.P.G.) and the School of Biomedical Sciences Bequest Fund from the University of Otago (to P.C.F., S.A.J., J.E.U. and P.P.G.). L.M.S. and L.M.M. were supported by University of Otago Doctoral Scholarships. We thank the staff of the Otago Micro and Nano Imaging facility for assistance with electron microscopy, M. Wilson for help with cell sorting and A. Jeffs of the Otago Genomics Facility for assistance with sequencing. We thank H. Hampton, A. Rey Campa, M. Yevstigneyeva and G. Salmond for providing strains and plasmids, and members of the Fineran laboratory for helpful discussions.

Author contributions

L.M.S. designed experiments, performed the SorTn-seq and the bioinformatic analyses, constructed plasmids and mutants, performed all reporter, interference, adaptation, phage adsorption and microscopy experiments, and prepared all the figures. S.A.J. designed experiments, performed bioinformatic analyses, constructed plasmids and provided supervision. L.M.M. generated strains and provided phages. J.E.U. provided supervision and input into the flow cytometry. P.P.G. assisted with bioinformatic analyses and supervision. P.C.F. conceptualized the study, designed experiments and supervised the project. L.M.S. and P.C.F. wrote the manuscript. All authors edited the manuscript.

Competing interests

The authors declare no competing interests.

Additional information

Extended data is available for this paper at https://doi.org/10.1038/s41564-020-00822-7.

Supplementary information is available for this paper at https://doi.org/10.1038/s41564-020-00822-7.

Correspondence and requests for materials should be addressed to P.C.F.

Peer review information *Nature Microbiology* thanks the anonymous reviewers for their contribution to the peer review of this work.

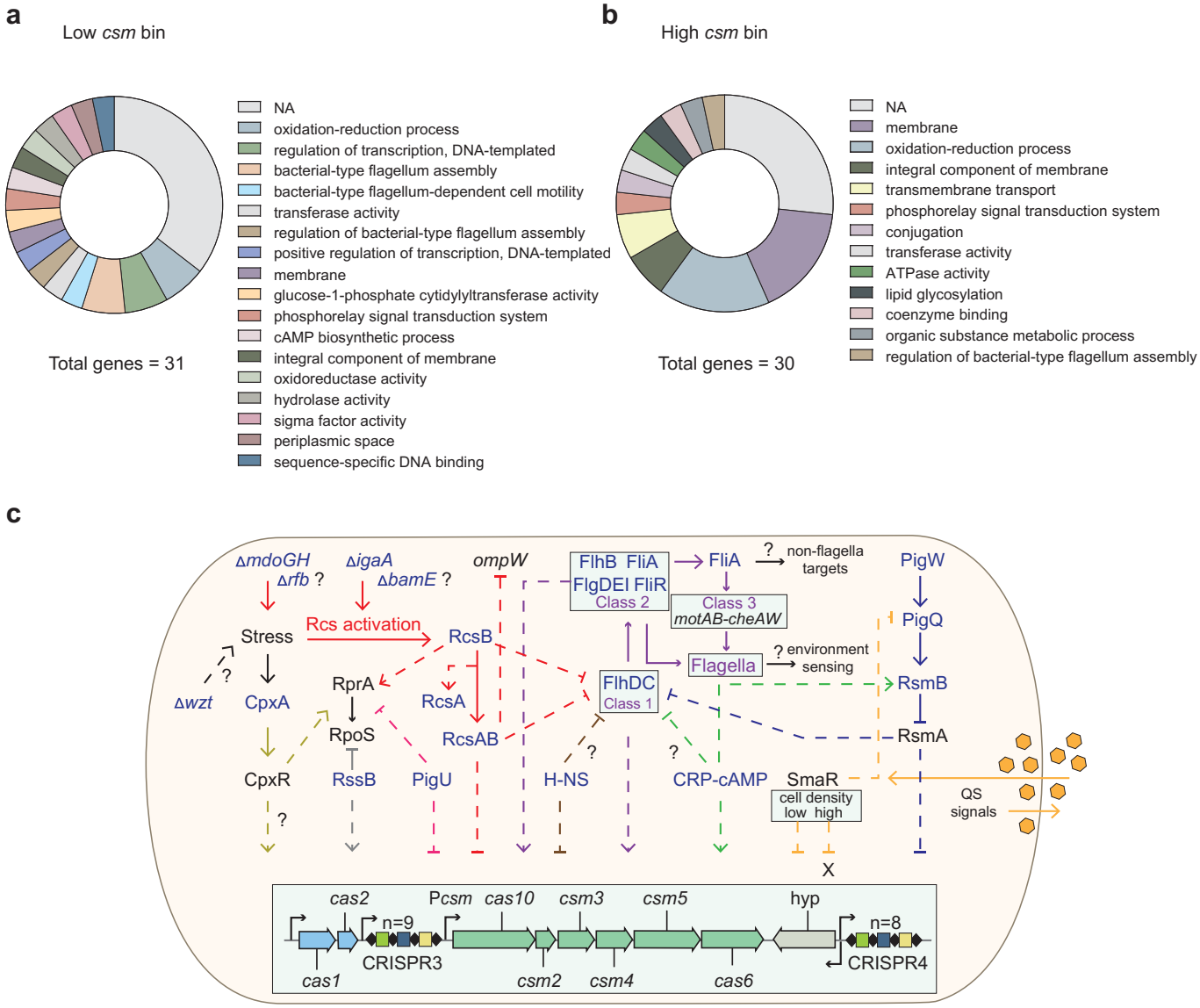

Extended Data Fig. 1 | Classification of significantly enriched genes and model of *csm* regulation in *Serratia*. a,b, Categories shown are Gene Ontology classifications[93,94] from the **a**, *low* expression bin and **b**, *high* expression bin. Locus tags and Gene Ontology information is detailed in Supplementary Table 2 (NA = no Gene Ontology term assigned). **c**, Main regulatory pathways controlling type III-A CRISPR-Cas immunity in *Serratia*. Features identified through *csm* SorTn-seq are shown in *dark blue*. Dashed lines indicate that the mechanism of regulation (direct versus indirect) is unknown. Connections between pathways that have been established in other organisms but have not yet been demonstrated in *Serratia* are indicated by a question mark (QS = quorum sensing).

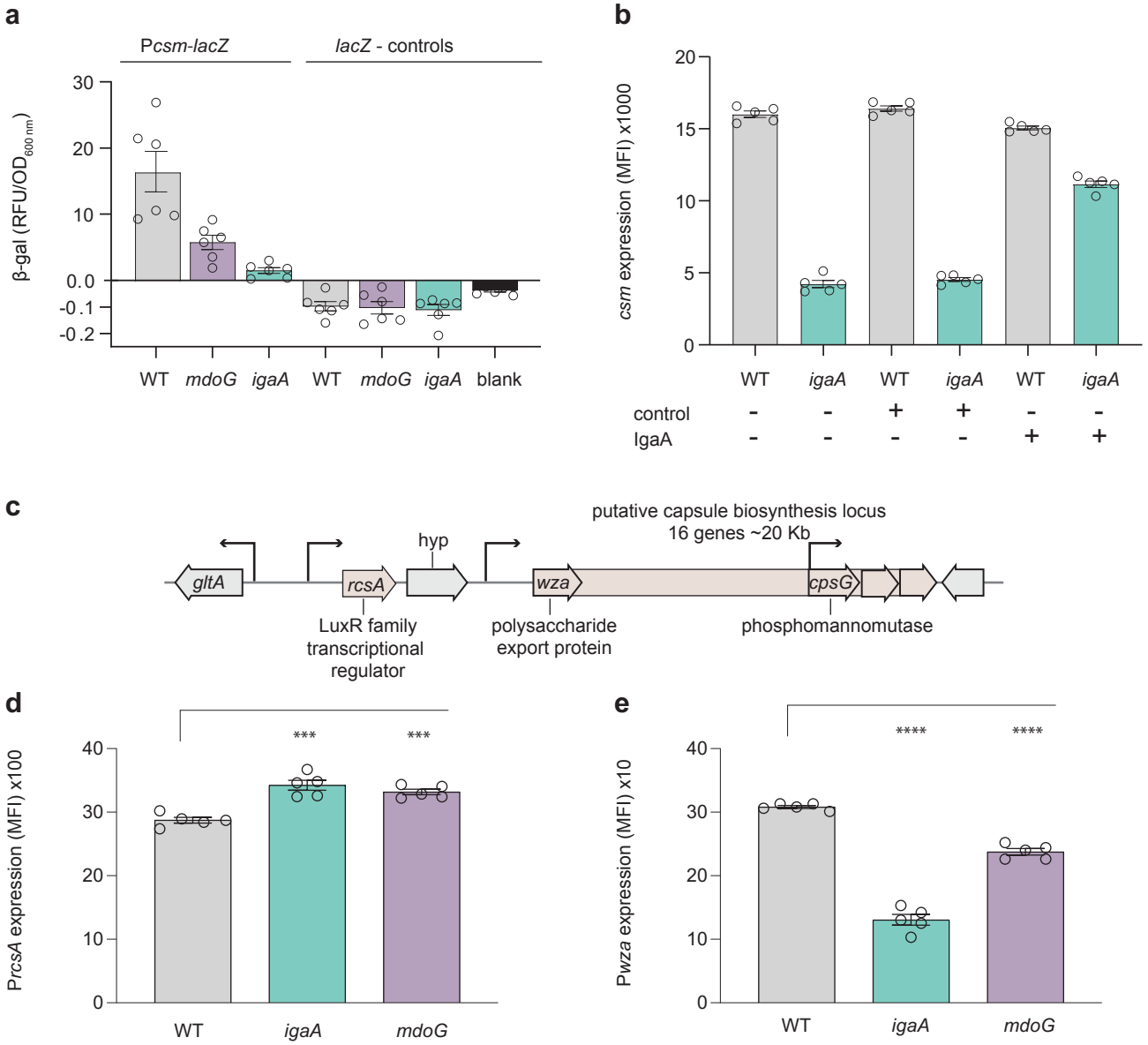

Extended Data Fig. 2 | Levels of *csm* expression and Rcs pathway-related promoters. a, Activity of the *csm* promoter was measured in strains containing a chromosomal LacZ reporter (P*csm-lacZ*) or no reporter controls (*lacZ*—controls) ($n = 6$ biologically independent samples). **b**, Expression of the *csm* promoter was partially restored in the *igaA* mutant background upon expression of *igaA* from a low copy number plasmid (pPF2143, RK2 origin; T5-lac promoter) versus control plasmid (pPF1622) ($n = 5$ biologically independent samples). MFI, median fluorescence intensity. **c**, Organization of a predicted capsular polysaccharide biosynthesis locus and predicted *rcsA* gene in *Serratia*. **d**, Expression levels of the *rcsA* promoter (P*rcsA*) is elevated in strains *igaA* and *mdoG*, which suggests positive autoregulation of *rcsA* upon Rcs-pathway induction ($n = 5$ biologically independent samples). **e**, Capsule locus expression, measured from a *wza* promoter fusion to *eYFP* (P*wza*), was reduced in Rcs-activated strains *igaA* and *mdoG*. The decrease in capsule locus expression is consistent with TEM imaging which showed no evidence of capsule synthesis in the *igaA* mutant ($n = 5$ biologically independent samples). All bars shown are the mean and error bars represent the s.e.m. For panels **d** and **e**, two-sided *t*-tests were used to determine statistical significance. Detailed statistical testing can be found in the accompanying Source Data file. $^{****}P < 0.0001$; $^{***}P < 0.001$.

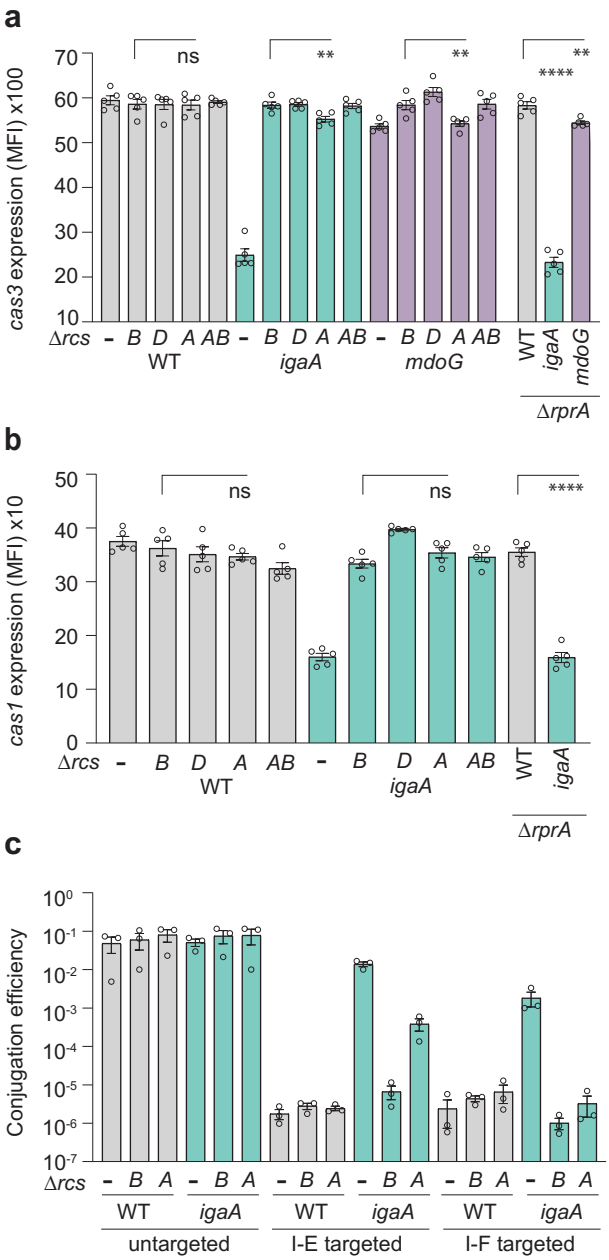

Extended Data Fig. 3 | See next page for caption.

Extended Data Fig. 3 | The Rcs pathway mediated changes in type I expression and interference. a, Repression of type I-E *cas3* expression requires *rcsB* in both strains *mdoG* and *igaA*, while *rcsA* contributes to repression only in strain *igaA*. The reduction of *cas3* expression is independent of *rprA* ($n = 5$ biologically independent samples). MFI, median fluorescence intensity. **b**, Repression of type I-F *cas1* expression requires both *rcsB* and *rcsA* in strain *igaA* and is independent of *rprA* ($n = 5$ biologically independent samples). **c**, CRISPR-Cas interference measured through conjugation efficiency of plasmids carrying protospacers matching endogenous CRISPR arrays (targeted) or control plasmids (untargeted). Type I-E CRISPR-Cas interference of the *igaA* strain is restored upon deletion of *rcsB*, and partially restored upon deletion of *rcsA* (I-E targeted). Type I-F interference levels of the *igaA* strain are restored upon deletion of *rcsB* or *rcsA* (I-F targeted). Conjugation efficiency of untargeted plasmids is similar amongst *rcsA* or *rcsB* deletions and isogenic parental strains (untargeted) ($n = 3$ biologically independent samples). All bars shown are the mean and error bars represent the s.e.m. For panels **a** and **b**, two-sided *t*-tests were used to determine statistical significance. Detailed statistical testing can be found in the accompanying Source Data file. $^{****}P < 0.0001$; $^{**}P < 0.01$; ns, not significant.

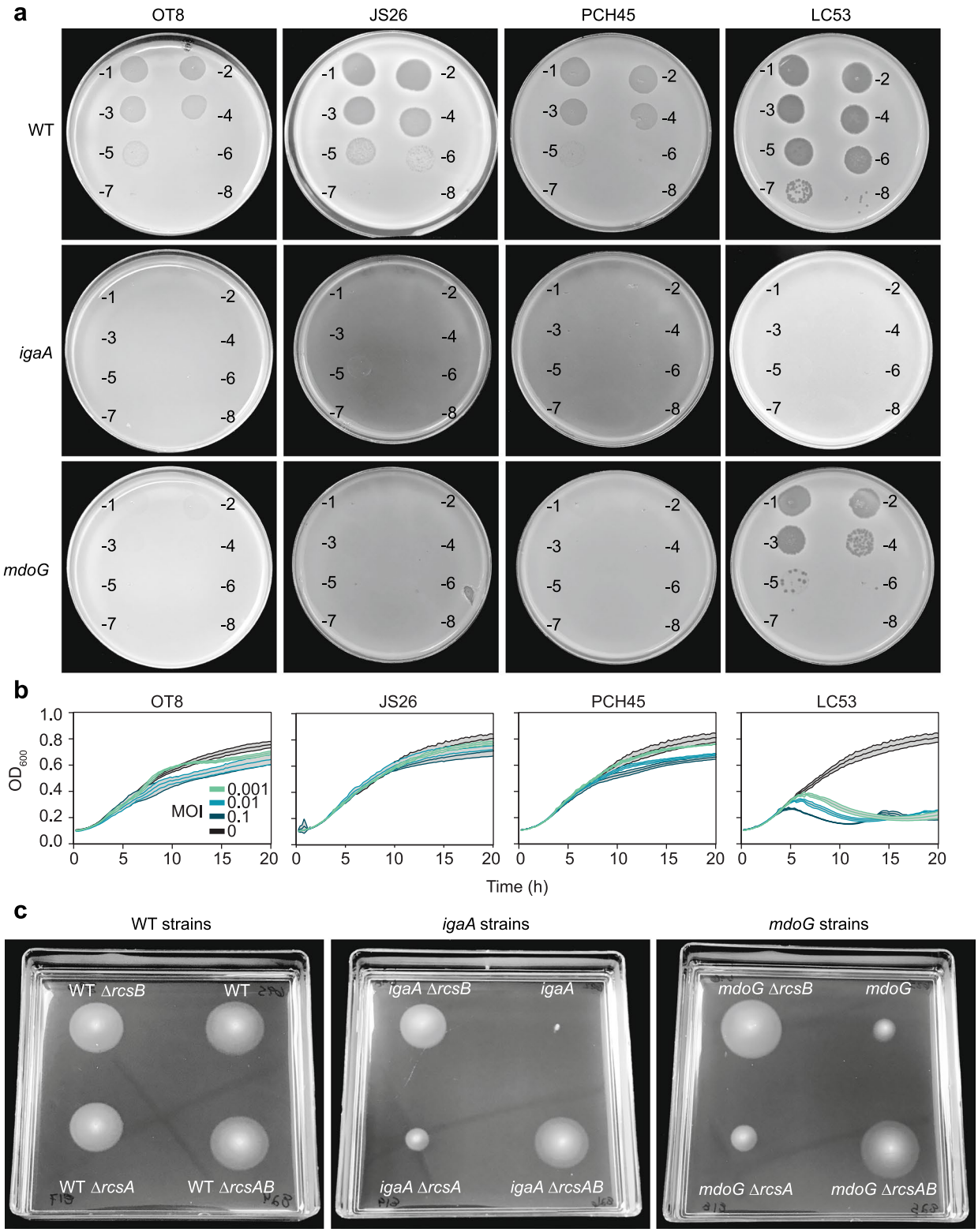

Extended Data Fig. 4 | Activation of the Rcs pathway results in attenuated phage infection and reduced swimming motility. a, During infection on plates, strain *igaA* is resistant to all phages. Faint clearing of the *mdoG* lawn is visible at high titers for flagellatropic phages OT8, JS26 and PCH45 (-1; ~10^9 PFU/ml and -2; ~10^8 PFU/ml). Infection of *mdoG* by LC53 is reduced on plates compared to WT. **b**, Strain *mdoG* is resistant to infection by flagellatropic phages in liquid, while remaining susceptible to phage LC53 ($n = 3$ biologically independent samples; lines represent the mean +/- the standard deviation). MOI, multiplicity of infection. **c**, Reduced swimming in *mdoG* and null swimming in *igaA* mutants is consistent with activation of the Rcs pathway. Deletion of *rcsB* (Δ*rcsB*) restores swimming motility to wild-type levels in *mdoG* and *igaA* mutant backgrounds, while deletion of the *rcsA* homolog RS09790 (Δ*rcsA*) does not. The partial restoration of swimming in strain *igaA* upon *rcsA* deletion is consistent with partial increase in *flhDC* expression (Extended Data Fig. 6), as well as partial re-sensitization to flagellatropic phages. (Extended Data Fig. 5). Deletion of both *rcsA* and *rcsB* (Δ*rcsAB*), results in similar swimming motility as the *rcsB* deletion.

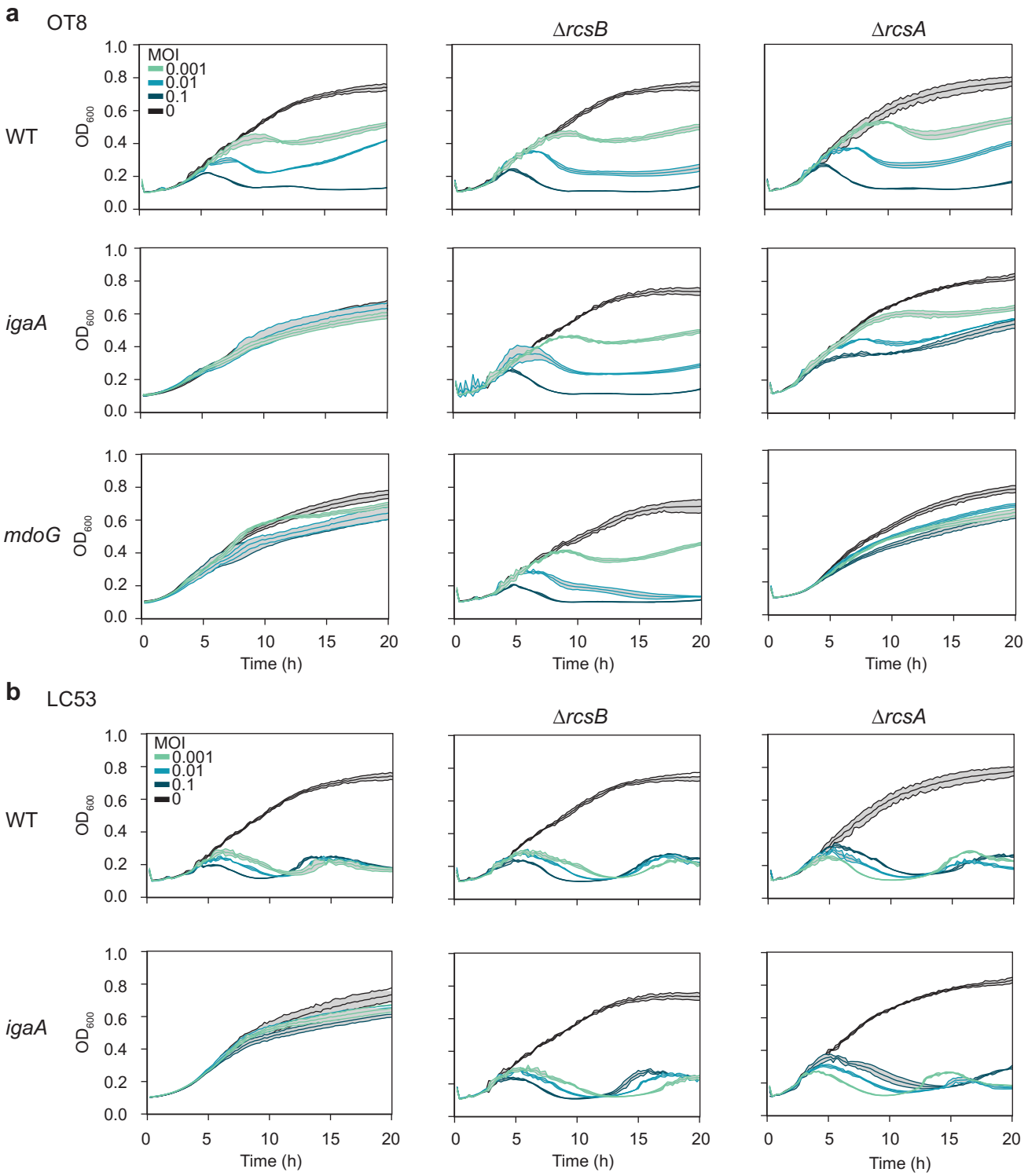

Extended Data Fig. 5 | Phage resistance in strains *igaA* and *mdoG* is dependent on the Rcs pathway. a, Deletion of *rcsB* restores susceptibility of strains *igaA* and *mdoG* to flagellatropic phage OT8. Deletion of *rcsA* partially sensitizes *igaA* to OT8, while *mdoG* remains largely resistant ($n = 3$ biologically independent samples). MOI, multiplicity of infection. These results support the partial role for *rcsA* in swimming motility (Extended Data Fig. 4) and flagella gene repression (Extended Data Fig. 6) observed in *igaA* but not *mdoG*. **b**, Deletion of either *rcsB* or *rcsA* restores susceptibility of strain *igaA* to phage LC53 resistant ($n = 3$ biologically independent samples). Lines in **a** and **b** represent the mean +/− the standard deviation.

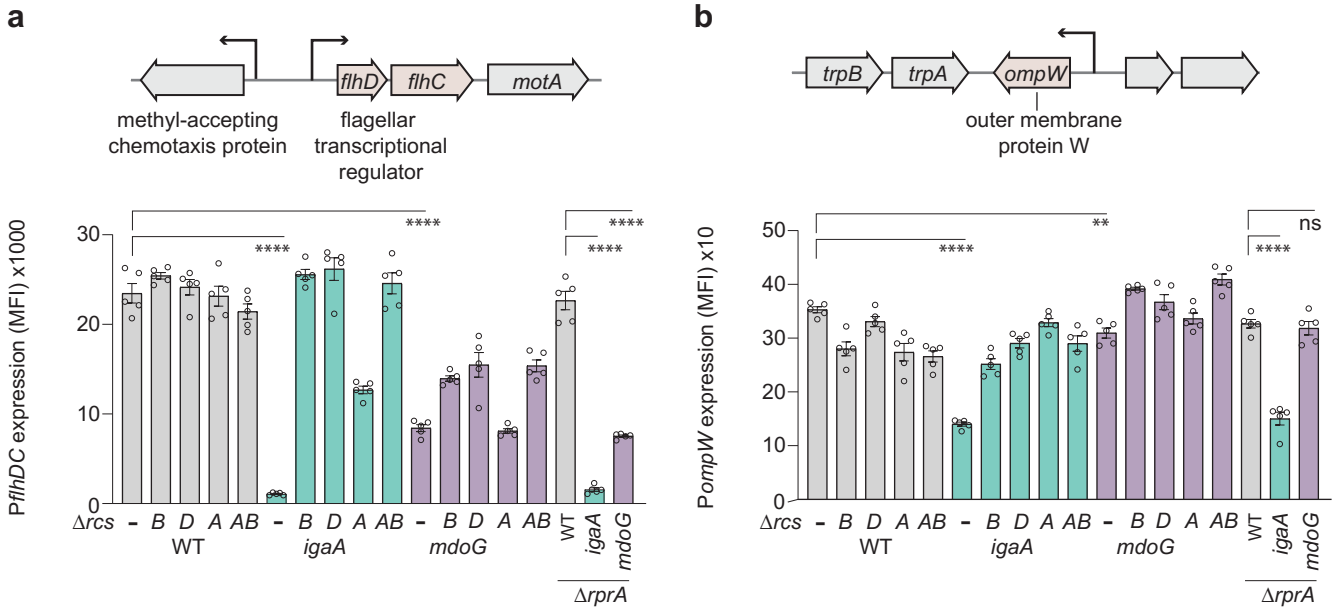

Extended Data Fig. 6 | Genetic organization and expression levels of Rcs-affected loci. a, Expression of the *flhDC* operon (flagella master regulator) promoter (P*flhDC*) is reduced in Rcs-activated strains. In strain *igaA*, restoration of expression to WT levels occurs upon deletion *rcsB* and *rcsD*, while *rcsA* deletion partially restores expression. Repression of P*flhDC* is independent of *rprA*. In *mdoG*, *flhDC* expression is increased upon deletion of *rcsB* and *rcsD* but is unaffected by *rcsA* deletion ($n = 5$ biologically independent samples). MFI, median fluorescence intensity. **b**, Expression of the *ompW* promoter (P*ompW*) is reduced in Rcs-activated strains. In strain *igaA*, an increase in expression is observed upon deletion *rcsB*, *rcsD*, or *rcsA*. In *mdoG*, the slight decrease in *ompW* expression does not alter phage LC53 infectivity in liquid but may contribute to an observed reduction in plaque formation on solid media (Extended Data Fig. 4). Repression of *ompW* is independent of *rprA* in the *igaA* mutant ($n = 5$ biologically independent samples). All bars indicate the mean and error bars represent the s.e.m. Two-sided *t*-tests were used to determine statistical significance. Detailed statistical testing can be found in the accompanying Source Data file. $^{****}P < 0.0001$; $^{**}P < 0.01$; ns, not significant.

nature research

Corresponding author(s): Peter C. Fineran

Last updated by author(s): Oct 21, 2020

Reporting Summary

Nature Research wishes to improve the reproducibility of the work that we publish. This form provides structure for consistency and transparency in reporting. For further information on Nature Research policies, see Authors & Referees and the Editorial Policy Checklist.

Statistics

For all statistical analyses, confirm that the following items are present in the figure legend, table legend, main text, or Methods section.

n/a	Confirmed	
☐	☒	The exact sample size (*n*) for each experimental group/condition, given as a discrete number and unit of measurement
☐	☒	A statement on whether measurements were taken from distinct samples or whether the same sample was measured repeatedly
☐	☒	The statistical test(s) used AND whether they are one- or two-sided *Only common tests should be described solely by name; describe more complex techniques in the Methods section.*
☒	☐	A description of all covariates tested
☐	☒	A description of any assumptions or corrections, such as tests of normality and adjustment for multiple comparisons
☐	☒	A full description of the statistical parameters including central tendency (e.g. means) or other basic estimates (e.g. regression coefficient) AND variation (e.g. standard deviation) or associated estimates of uncertainty (e.g. confidence intervals)
☐	☒	For null hypothesis testing, the test statistic (e.g. *F*, *t*, *r*) with confidence intervals, effect sizes, degrees of freedom and *P* value noted *Give P values as exact values whenever suitable.*
☒	☐	For Bayesian analysis, information on the choice of priors and Markov chain Monte Carlo settings
☒	☐	For hierarchical and complex designs, identification of the appropriate level for tests and full reporting of outcomes
☒	☐	Estimates of effect sizes (e.g. Cohen's *d*, Pearson's *r*), indicating how they were calculated

Our web collection on statistics for biologists contains articles on many of the points above.

Software and code

Policy information about availability of computer code

Data collection	Flow cytometry data was collected using BD FACSDiva software (version 8; BD Biosciences) on a FACSAria Fusion or LSRFortessa (BD Biosciences) for fluorescence activated cell sorting or flow cytometry, respectively. Phage infection curve data was measured using a Varioskan Flash plate reader and SkanIt software (Thermo Scientific).
Data analysis	Flow cytometry data was analyzed using FlowJo software (version 10; BD Biosciences). Quality control of Illumina sequencing libraries was performed using the QuantStudio Real-Time PCR software (Thermo Scientific) for qPCR data, and 2100 Expert software (Agilent) for Bioanalyzer data. Illumina sequencing reads were processed using the BioTradis pipeline (https://github.com/sanger-pathogens/Bio-Tradis) to generate plot files, summarizing reads per nucleotide position of the reference genome (per sample). Plot files were further analyzed using custom R scripts which are available on GitHub (https://github.com/JacksonLab/SorTn-seq). Statistical analyses (apart from Illumina sequencing data) were performed using GraphPad Prism (version 8).

For manuscripts utilizing custom algorithms or software that are central to the research but not yet described in published literature, software must be made available to editors/reviewers. We strongly encourage code deposition in a community repository (e.g. GitHub). See the Nature Research guidelines for submitting code & software for further information.

Data

Policy information about availability of data

All manuscripts must include a data availability statement. This statement should provide the following information, where applicable:

- Accession codes, unique identifiers, or web links for publicly available datasets
- A list of figures that have associated raw data
- A description of any restrictions on data availability

The data that support the findings of this study are available from the corresponding author upon request. Sequencing data is available in the SRA under BioProject number PRJNA601789. The annotated genome of Serratia sp. ATCC 39006 - LacA is available under NCBI reference sequence NZ_CP025085.1 (https://www.ncbi.nlm.nih.gov/nuccore/NZ_CP025085.1).

Field-specific reporting

Please select the one below that is the best fit for your research. If you are not sure, read the appropriate sections before making your selection.

☒ Life sciences ☐ Behavioural & social sciences ☐ Ecological, evolutionary & environmental sciences

For a reference copy of the document with all sections, see nature.com/documents/nr-reporting-summary-flat.pdf

Life sciences study design

All studies must disclose on these points even when the disclosure is negative.

Sample size	No statistical methods were used to predetermine sample size. Each experiment had at least 3 independent biological replicates as is standard in the microbiology field. Large differences were observed in most cases, so small samples sizes were sufficient.
Data exclusions	No data points were excluded from analyses.
Replication	Reproducibility of our experiments was determined by performing experiments with at least 3 biological replicates and we observed reproducible data. Expression and conjugation efficiency experiments were repeated a minimum of two times (each with at least 3 biological replicates), with reproducible results.
Randomization	Any microbiological cultures subjected to different treatments (e.g. +/- phage infection) were randomly assigned to each group.
Blinding	The datasets used in the main study were generated using quantitative processes (e.g. cell-sorting, high-throughput sequencing, bioinformatic analysis). The authors had no influence over the outcomes of these experiments beyond the initial conditions. Therefore blinding is not relevant to the study design.

Reporting for specific materials, systems and methods

We require information from authors about some types of materials, experimental systems and methods used in many studies. Here, indicate whether each material, system or method listed is relevant to your study. If you are not sure if a list item applies to your research, read the appropriate section before selecting a response.

Materials & experimental systems

n/a	Involved in the study
☒	☐ Antibodies
☒	☐ Eukaryotic cell lines
☒	☐ Palaeontology
☐	☒ Animals and other organisms
☒	☐ Human research participants
☒	☐ Clinical data

Methods

n/a	Involved in the study
☒	☐ ChIP-seq
☐	☒ Flow cytometry
☒	☐ MRI-based neuroimaging

Animals and other organisms

Policy information about studies involving animals; ARRIVE guidelines recommended for reporting animal research

Laboratory animals	The study did not involve laboratory animals.
Wild animals	The study did not involve wild animals.
Field-collected samples	This study did not involve field-collected samples.
Ethics oversight	No ethical approval was required.

Note that full information on the approval of the study protocol must also be provided in the manuscript.

Flow Cytometry

Plots

Confirm that:

☒ The axis labels state the marker and fluorochrome used (e.g. CD4-FITC).

☒ The axis scales are clearly visible. Include numbers along axes only for bottom left plot of group (a 'group' is an analysis of identical markers).

☒ All plots are contour plots with outliers or pseudocolor plots.

☒ A numerical value for number of cells or percentage (with statistics) is provided.

Methodology

Sample preparation	For fluorescence activated cell sorting, one ml aliquots of frozen transposon mutant library were subcultured (starting OD600 = 0.05) into 30 ml LB with chloramphenicol for reporter plasmid selection, kanamycin for transposon selection, and Isopropyl β-d-1-thiogalactopyranoside (IPTG) for mCherry induction. Cells were grown for 16 h to allow expression of the Pcsm-eYFP reporter. Prior to sorting, 1 ml of culture was removed for DNA extraction to serve as the input library. Cells were then diluted in 15 ml PBS (1:30) for sorting. For expression analysis, cells were grown for 20 h in 1 ml LB with appropriate supplements in a 96 deep well plate (Labcon) at 30°C with shaking at 1200 rpm in an IncuMix incubator shaker (Select BioProducts). Cells were diluted in PBS (1:1000 or adjusted when necessary) prior to sample measurement.
Instrument	Cell sorting was performed using a FACSAria Fusion (BD Biosciences) and expression analyses was performed using a LSRFortessa (BD Biosciences).
Software	BD FACSDiva software (version 8; BD Biosciences) and FlowJo software (version 10; BD Biosciences).
Cell population abundance	The frequency of cells falling within the "sorting" gate was (on average) 38% of the total ungated cell population. Cells within this gate were sorted three-ways into different expression bins/pools: low (bottom ~5% of fluorescence distribution), depleted (middle ~90%), and high (top 5%). Cells were sorted into PBS and gDNA was extracted from sort pools for subsequent transposon sequencing.
Gating strategy	For fluorescence activated cell sorting, cells were first gated on parameters of forward scatter (FSC) and side scatter (SSC) area (A) and height (H) to isolate single cells (FSC-H/FSC-A; SSC-A/SSC-H; FSC-A/SSC-A). Cells within the FSC-A/SSC-A gate were further gated in a final "sorting" gate, to include only cells with positive mCherry (YG_610_20-A) and eYFP fluorescence (B_530_30-A). For expression analysis and plasmid clearance assays, cells were first gated on SSC-H/SSC-A and FSC-A/SSC-A, then further gated into mCherry (YG_610_20-A) positive and negative populations. For plasmid clearance experiments, the percentage of mCherry negative cells (YG_610_20-A-) relative to total cells within gate FSC-A/SSC-A is reported. For expression analysis, eYFP expression (B_530_30-A median fluorescence intensity) was measured from the mCherry positive (YG_610_620-A+) gate. PMT voltages were adjusted such that non-fluorescent cell populations (controls) had a median fluorescence intensity of approximately zero. We generally observed a 2-3-log separation between fluorescent and non-fluoresecent populations which aided in delineating positive and negative populations.

☒ Tick this box to confirm that a figure exemplifying the gating strategy is provided in the Supplementary Information.